Article

TRANSPARENT PROCESS

THE EMBO JOURNAL

Gut colonization by *Bacteroides* requires translation by an EF-G paralog lacking GTPase activity

Weiwei Han[1,2], Bee-Zen Peng[3], Chunyan Wang[1,2], Guy E Townsend II[1,2,†], Natasha A Barry[1,2], Frank Peske[3], Andrew L Goodman[1,2], Jun Liu[1,2], Marina V Rodnina[3] & Eduardo A Groisman[1,2,*]

Abstract

Protein synthesis is crucial for cell growth and survival yet one of the most energy-consuming cellular processes. How, then, do cells sustain protein synthesis under starvation conditions when energy is limited? To accelerate the translocation of mRNA–tRNAs through the ribosome, bacterial elongation factor G (EF-G) hydrolyzes energy-rich guanosine triphosphate (GTP) for every amino acid incorporated into a protein. Here, we identify an EF-G paralog—EF-G2—that supports translocation without hydrolyzing GTP in the gut commensal bacterium *Bacteroides thetaiotaomicron*. EF-G2's singular ability to sustain protein synthesis, albeit at slow rates, is crucial for bacterial gut colonization. EF-G2 is ~10-fold more abundant than canonical EF-G1 in bacteria harvested from murine ceca and, unlike EF-G1, specifically accumulates during carbon starvation. Moreover, we uncover a 26-residue region unique to EF-G2 that is essential for protein synthesis, EF-G2 dissociation from the ribosome, and responsible for the absence of GTPase activity. Our findings reveal how cells curb energy consumption while maintaining protein synthesis to advance fitness in nutrient-fluctuating environments.

Keywords *Bacteroides thetaiotaomicron*; elongation factor G; GTP hydrolysis; paralogous proteins; ribosome

Subject Categories Microbiology, Virology & Host Pathogen Interaction; Translation & Protein Quality

DOI 10.15252/embj.2022112372 | Received 15 August 2022 | Revised 11 November 2022 | Accepted 11 November 2022 | Published online 6 December 2022

The EMBO Journal (2023) 42: e112372

Introduction

Protein synthesis is carried out by the ribosome. Following incorporation of each amino acid into a growing polypeptide chain, the ribosome moves by three nucleotides along the mRNA. The two tRNAs bound to the A and P sites of the ribosome move to the P and E sites, respectively, exposing a new codon in the A site. This movement—referred to as translocation—can happen spontaneously but is accelerated by four orders of magnitude in the presence of specific translation factors essential in all living cells. These translation factors—elongation factor G (EF-G) in prokaryotes and elongation factor 2 (EF2) in eukaryotes—are guanosine triphosphate (GTP)-hydrolases (GTPases) that use the energy derived from GTP hydrolysis to accelerate translocation (Rodnina *et al*, 2019). EF-G also functions with ribosome recycling factor (RRF) to promote the rapid dissociation of the ribosomal complex into the small and large subunits after release of the synthetized protein, also at the cost of GTP hydrolysis (Hirashima & Kaji, 1973; Peske *et al*, 2005). Here, we present the first example of an EF-G that sustains protein synthesis without consuming GTP and establish that this ability is critical for bacterial colonization of the mammalian gut.

Members of the *Bacteroidetes* (*Bacteroidota*) phylum, especially the *Bacteroides* genus, make up a major portion of the human gut microbiota and are widespread across human populations (Wexler & Goodman, 2017). *Bacteroides* species are obligate anaerobes highly adapted to life in the gut as they live and grow exclusively in the gastrointestinal tracts of mammals (Ley *et al*, 2008). They are the foundation of the microbial food webs in the gut because they can break down a wide range of complex sugars (including dietary plant polysaccharides, host glycans, and milk oligosaccharides) that are major carbon sources (Martens *et al*, 2014; Schwalm III & Groisman, 2017; La Rosa *et al*, 2022). Nevertheless, *Bacteroides* species appear to experience carbon limitation in the gut because proteins and signaling molecules that accumulate upon carbon starvation are required for gut colonization (Schofield *et al*, 2018; Townsend II *et al*, 2020). This raises the question: How do *Bacteroides* species sustain protein synthesis under energy-limiting conditions?

Bacteroides thetaiotaomicron harbors two EF-G-like proteins: the essential EF-G1 (BT2729), which shares 57% amino acid identity (73% similarity, Fig EV1A) with the canonical *Escherichia coli* EF-G, and EF-G2 (BT2167), which shares 34% amino acid identity (53% similarity, Fig EV1A) with *E. coli* EF-G. EF-G1 and EF-G2 share 31% amino acid identity and 51% amino acid similarity (Fig EV1A). EF-G2 is required for successful colonization of the murine gut (Wu *et al*, 2015; Townsend II *et al*, 2020) but dispensable under laboratory conditions. When *B. thetaiotaomicron* experiences carbon limitation, the mRNA amounts of the canonical EF-G1 (*BT2729*) gene

1 Department of Microbial Pathogenesis, Yale School of Medicine, New Haven, CT, USA
2 Yale Microbial Sciences Institute, West Haven, CT, USA
3 Department of Physical Biochemistry, Max Planck Institute for Multidisciplinary Sciences, Göttingen, Germany
*Corresponding author. Tel: +1 314 495 5802; E-mail: eduardo.groisman@yale.edu
†Present address: Department of Biochemistry and Molecular Biology, Penn State College of Medicine, Hershey, PA, USA

© 2022 The Authors.

decrease ~10-fold (Townsend II *et al*, 2020), which is consistent with translational shut-down under starvation conditions and makes sense given that protein synthesis is the most energy-demanding cellular activity and that carbon starvation dramatically reduces energy production. By contrast, the mRNA amounts of the EF-G2 (*BT2167*) gene increase > 200-fold during carbon limitation (Townsend II *et al*, 2020). That EF-G1 is essential but EF-G2 is not distinguishes *B. thetaiotaomicron* from bacterial species that harbor two essential EF-G-like proteins, one responsible for translocation and the other responsible for ribosome recycling (Suematsu *et al*, 2010; Margus *et al*, 2011).

Here, we identify *B. thetaiotaomicron* EF-G2 as the first natural EF-G protein that promotes translation elongation without GTP hydrolysis. We determine that EF-G2 does not hydrolyze GTP in the presence of pre-translocation ribosome complexes or ribosomes without bound tRNAs or mRNA (vacant ribosomes) even though EF-G2 binds GTP more tightly than the canonical *B. thetaiotaomicron* EF-G1. Cryo-electron microscopy analysis reveals that the GTP-binding pocket of EF-G2 is located further away from the sarcin-ricin loop of the ribosome than in complexes with canonical EF-G proteins, which may account for the lack of ribosome-stimulated GTPase activity in EF-G2. An engineered *B. thetaiotaomicron* strain with a translocation-deficient EF-G2 variant replacing wild-type EF-G2 is as defective in gut colonization as an EF-G2 null mutant. Taken together with the high abundance of EF-G2 in bacteria harvested from murine ceca that contrasts with the exceedingly low amounts of EF-G1, this indicates that protein synthesis mediated by EF-G2 is essential for gut colonization. Our findings reveal how paralogous translation factors enable commensal bacteria to switch from rapid energy-consuming protein synthesis to a slower energy-efficient process, advancing bacterial fitness in nutrient-fluctuating environments.

Results

EF-G2 is well conserved across the *Bacteroides* genus and displays unique sequence signatures

Phylogenetic analysis of the EF-G1- and EF-G2-encoding genes suggests that they originated from ancestral duplicated genes that likely existed in the last common ancestor of bacteria (Atkinson, 2015). EF-G2-encoding genes have been identified in every bacterial phylum but only in about one fourth of the species (Margus *et al*, 2011). Notably, EF-G2 never exists as the sole EF-G-like protein in any organism, being always accompanied by either an ortholog of canonical EF-G or both spdEF-G1 and spdEF-G2, which are EF-G-paralogs specialized in translocation and ribosome recycling, respectively, and present in *Spirochaetes*, *Planctomycetes*, and *Delta-proteobacteria* in place of canonical EF-G (Suematsu *et al*, 2010; Margus *et al*, 2011). The scattered distribution of EF-G2-specifying genes in currently available genomes may have resulted from gene loss in some lineages during evolution. The deduced amino acid sequences of the extant EF-G2 proteins reveal more divergence than EF-G proteins, harboring lineage-specific motifs and insertions/deletions (Margus *et al*, 2011) that may confer lineage-specific functions. One such function(s) is likely responsible for EF-G2 being required for colonization of the mammalian gut by three different *Bacteroides* species: *B. thetaiotaomicron*, *B. cellulosilyticus*, and *B. ovatus* (Wu *et al*, 2015). This prompted us to investigate the conservation of EF-G2 in the *Bacteroides* lineage.

Genome analysis revealed that genes specifying EF-G2 are present in all 71 analyzed fully sequenced genomes from the *Bacteroides* genus, with the corresponding amino acid sequences sharing 75–100% identity with the *B. thetaiotaomicron* EF-G2 protein (Fig 1A). Outside the *Bacteroides* genus, EF-G2-specifying genes share lower deduced amino acid sequence identity (60–80% in *Bacteroidaceae* and 48–60% in the rest of *Bacteroidetes*) with the *B. thetaiotaomicron* EF-G2 (Fig 1A). Of the 146 genomes from the *Bacteroidia* class analyzed, only two lack an EF-G2-specifying gene (Fig 1A). By contrast, an EF-G2-specifying gene is found in a smaller portion of *Bacteroidetes* outside the *Bacteroidia* class (10/197 *Flavobacteriia*, 2/30 *Sphingobacteriia*, 3/100 *Cytophagia*, 19/29 *Chitinophagia*, 61/81 *Saprospiria* genomes analyzed).

All *Bacteroides* EF-G2 proteins harbor the conserved glutamine Q507 and histidine H583 residues (*E. coli* EF-G numbering; Figs 1B and C, and EV1A), which contact tRNA and are critical for translocation by EF-G (Savelsbergh *et al*, 2000; Gao *et al*, 2009). These residues are conserved in EF-G orthologs, EF-G2 proteins, and spdEF-G1 but not in the translocation-incompetent spdEF-G2 (Fig EV1A; Margus *et al*, 2011).

A distinguishing feature of *Bacteroides* EF-G2 is the presence of a 26-amino acid long insert in domain IV found neither in EF-G proteins nor in EF-G2 proteins from bacteria outside the *Bacteroidetes*

Figure 1. EF-G2 is well conserved across the *Bacteroides* genus.

A Phylogenetic tree of 149 whole-genome sequenced strains from the *Bacteroidetes* phylum, including 71 *Bacteroides* spp. strains (light blue background), with the blue-yellow heatmap showing the presence of EF-G1 or EF-G2 sequelog, and the identity between each homolog and the corresponding *B. thetaiotaomicron* VPI-5482 protein; the ring of letters (aa84) shows amino acid at the position 84 (*B. thetaiotaomicron* EF-G2 numbering) of corresponding EF-G2 proteins; and the outermost bar-charts [Insert (bp)] shows the length of the insert corresponding to residues 514–539 in *B. thetaiotaomicron* EF-G2. Background colors: blue—*Bacteroides* genus; purple—*Bacteroidaceae* family; gray—*Bacteroidales* order, *Bacteroidia* class. The three listed *Bacteroidetes* lacking EF-G2 sequelogs are: *Flavobacterium johnsoniae*, which is a soil bacterium; *Candidatus Azobacteroides pseudotrichonymphae*, which was isolated from a single cell of the protist *Pseudotrichonympha grassii*, which resides in the termite gut; *Porphyromonas* sp. *KLE 1280*, which is a human oral bacterium.

B, C Sequence logos of the aligned deduced amino acid sequences of the EF-G1 and EF-G2 proteins from *Bacteroides* species showing the regions corresponding to Loop I (B) and Loop II (C) at the tip of domain IV in canonical EF-G. Only unique (non-redundant) protein sequences were used for the alignment.

D Sequence logos of aligned deduced amino acid sequences of EF-G1 and EF-G2 proteins from *Bacteroides* species showing the region surrounding the EF-G2 insert with amino acids that form beta-strand and beta-hairpin in *B. thetaiotaomicron* EF-G2 shown by arrows below the logos.

E Sequence logos of aligned deduced amino acid sequences of EF-G1 and EF-G2 proteins from *Bacteroides* species showing the G3-box (DTPG in canonical EF-G) followed by the conserved histidine in *Bacteroides* EF-G1s and the corresponding serine/alanine in *Bacteroides* EF-G2s. The *B. thetaiotaomicron* EF-G2 has a serine at this position (S84).

 © 2022 The Authors

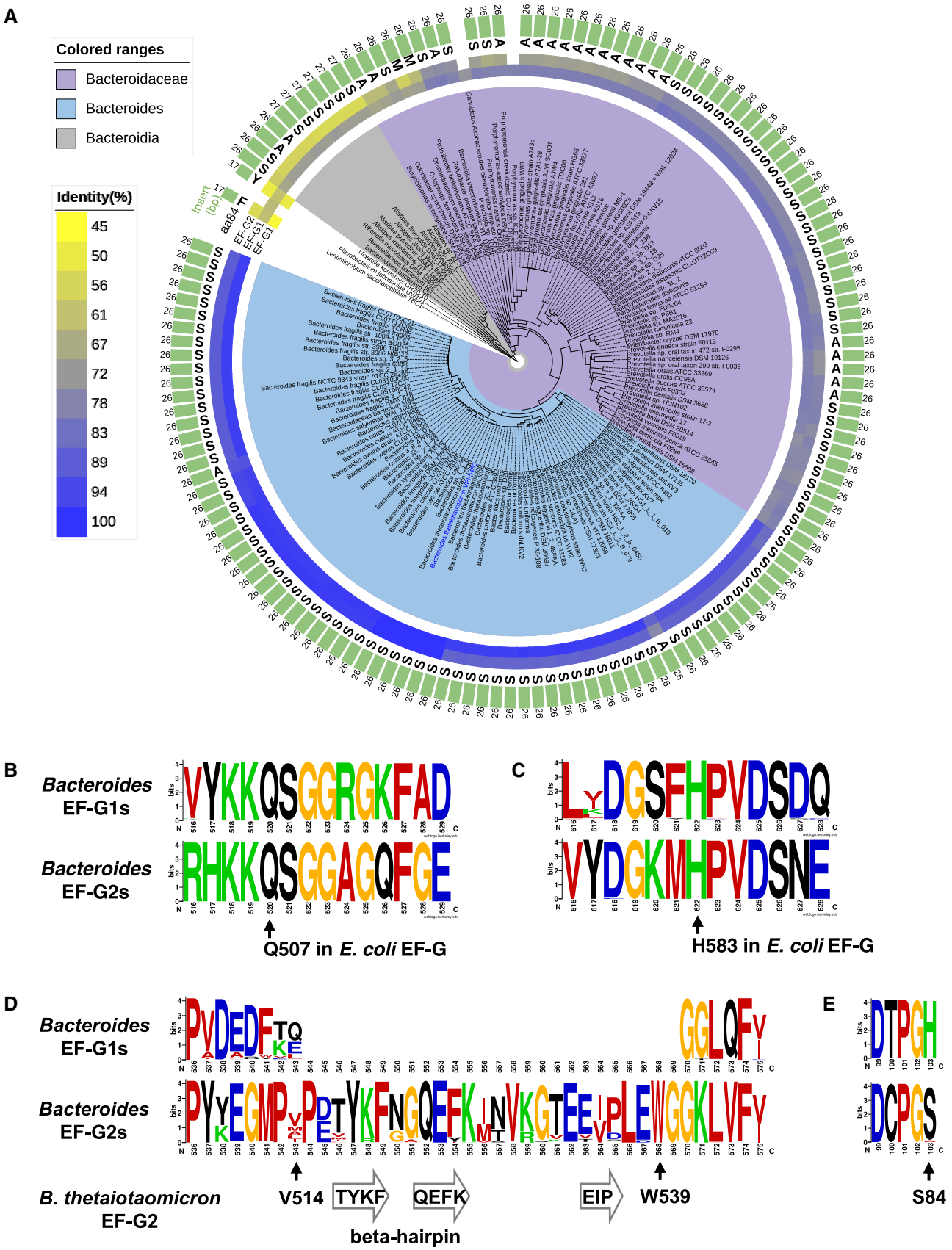
A
Colored ranges
Bacteroidaceae
Bacteroides
Bacteroidia
Identity(%)
45
50
56
61
67
72
78
83
89
94
100
Insert (bp)
aa84
EF-G2
EF-G1
EF-G1
B
Bacteroides EF-G1s
Bacteroides EF-G2s
Q507 in E. coli EF-G
C
H583 in E. coli EF-G
D
Bacteroides EF-G1s
Bacteroides EF-G2s
B. thetaiotaomicron EF-G2
V514
TYKF
QEFK
EIP
W539
beta-hairpin
E
S84

Figure 1.

phylum (Fig EV1A; Margus *et al*, 2011). The insert is shared by all *Bacteroides* EF-G2 proteins, having the same length and well-conserved amino acid sequence (Fig 1D). By contrast, EF-G2 proteins from *Bacteroidetes* outside the *Bacteroidia* class harbor a shorter 17 residue-long insert (Figs 1A and EV1B).

Curiously, histidine H91 (*E. coli* EF-G numbering), which is conserved in EF-G orthologs (Fig EV1A) as well as in other translational GTPases, including EF-Tu, RF3, LepA, and IF2, is not conserved in EF-G2 proteins, being substituted by either a serine (S84 in *B. thetaiotaomicron* EF-G2) or an alanine in *Bacteroides* EF-G2 proteins (Fig 1E). An earlier study of a more limited number of genomes reported that the consensus amino acid at this position of EF-G2 is serine in the *Bacteroidetes* phylum and *Alphaproteobacteria* and *cyanobacteria* groups, leucine in *Chlorobi*, and phenylalanine or tyrosine in other groups of bacteria (Margus *et al*, 2011). We noticed that EF-G2s from the *Bacteroidia* class harbor serine, alanine, or methionine at this position and that EF-G2s from the other classes of *Bacteroidetes* harbor tyrosine, phenylalanine, or leucine (Figs 1A and EV1B). Despite harboring a tyrosine at this position, the *Thermus thermophilus* EF-G2 is active in GTP-hydrolysis and translation elongation (Connell *et al*, 2007). By contrast, an *E. coli* EF-G variant with the H91A substitution is inactive in both GTP hydrolysis and translation elongation but can support a single round of slow tRNA–mRNA translocation (Cunha *et al*, 2013). This prompted us to determine whether EF-G2 from *B. thetaiotaomicron* is a functional translation factor.

EF-G2 is a *bona fide* translation elongation factor that promotes slow translocation

To determine whether EF-G2 can support protein synthesis, we used an *in vitro* reconstituted custom-made protein synthesis system (PURExpress, New England Biolabs) containing a defined mix of purified *E. coli* transcription and translation components except for EF-G. Recombinant *B. thetaiotaomicron* EF-G2 purified from *E. coli* promoted synthesis of a reporter protein specified by the provided DNA template (Fig 2A), albeit more slowly than recombinant *B. thetaiotaomicron* EF-G1 purified under the same conditions (Fig 2A). EF-G1 exhibited similar activity to *E. coli* EF-G (Fig 2A), validating the approach of using the *E. coli*-based system to study *B. thetaiotaomicron* EF-G proteins.

Control experiments verified that the observed protein synthesis is mediated by the added EF-G proteins. First, no reporter protein was produced in the absence of *E. coli* EF-G, EF-G1, or EF-G2 (Fig 2A), indicating that the protein synthesis system was free of endogenous *E. coli* EF-G. Second, the *B. thetaiotaomicron* EF-G2 (H593K) mutant protein, purified using the same method as for purification of wild-type EF-G2, was inactive in protein synthesis (Fig 2A). H593 in *B. thetaiotaomicron* EF-G2 corresponds to H583 in *E. coli* EF-G (Fig EV1A), a histidine residue which upon substitution to lysine renders EF-G unable to support rapid translocation (Savelsbergh *et al*, 2000). The inability of the purified EF-G2 (H593K) variant to sustain protein synthesis indicates that the protein synthesis activity conferred by recombinant wild-type EF-G2 is unlikely to result from contamination with endogenous *E. coli* EF-G from the bacterial host used to overproduce the *B. thetaiotaomicron* EF-G2 protein.

We then tested whether the slower rate of protein synthesis conferred by EF-G2 relative to EF-G1 (Fig 2A) is due to slower tRNA–mRNA translocation in the presence of EF-G2. We measured translocation kinetics in a fully reconstituted translation system using an established stopped-flow assay that monitors the fluorescence change of fluorescein attached to the 3′ end of a short mRNA upon translocation (Savelsbergh *et al*, 2003). The experiments were carried out in the presence of excess EF-G, which allowed us to capture the effect on translocation independently of the subsequent EF-G dissociation step. In the presence of GTP, EF-G2-mediated translocation was significantly slower than that mediated by EF-G1 (0.7 ± 0.1 s^{-1} vs. 6.9 ± 0.2 s^{-1}; Fig 2B), which was as fast as that supported by *E. coli* EF-G (Fig EV2A). EF-G2's behavior is reminiscent of that exhibited by the GTPase-deficient *E. coli* EF-G (H91A) variant (Cunha *et al*, 2013). In agreement with this notion, translocation carried out with EF-G1 in the presence of the non-hydrolysable GTP analog GDPNP (guanosine 5′-[β,γ-imido] triphosphate; Fig 2B) was much slower than in the presence of GTP (Fig 2B) and resembled the kinetics of EF-G2-promoted translocation in the presence of either GDPNP or GTP (Fig 2B). Moreover, the fluorescence change in the reaction with EF-G2 reached a lower amplitude than that in reactions with EF-G1 or *E. coli* EF-G (Figs 2B and EV2A). The lower fluorescence amplitude, which is also observed with *E. coli* EF-G in the presence of other non-hydrolysable GTP analogs (Belardinelli *et al*, 2016), is due to the inhibition of 30S ribosomal subunit movements, namely the impaired swivel motion of the head domain of the 30S ribosomal subunit back to the ground state (Belardinelli *et al*, 2016). The ribosomes are blocked in an intermediate state (termed chimeric) with the mRNA fully translocated relative to the body domain of the 30S subunit, whereas translocation on the head domain is incomplete, which leads to an incomplete fluorescence amplitude with mRNA reporters.

To further characterize translocation in the presence of EF-G2, we monitored formation of a tripeptide upon addition of EF-G to ribosome initiation complexes, aminoacyl-tRNA:EF-Tu:GTP ternary complexes, and GTP (Peng *et al*, 2019). After formation of the first peptide bond (which is independent of translocation), binding of the second aminoacyl-tRNA:EF-Tu:GTP can occur only if tRNA–mRNA translocation is completed and EF-G has dissociated from the ribosome. EF-G2 promoted complete translocation to an extent comparable to that with EF-G1 or *E. coli* EF-G (Fig 2C), but with a much lower rate, about 0.004 s^{-1} (Fig 2C, inset). This is much slower than the dissociation of *E. coli* EF-G, about 4 s^{-1} (Belardinelli *et al*, 2016), or the mRNA translocation in the presence of EF-G2 measured with the translocation assay in Fig 2B (0.7 s^{-1}). Because formation of the tripeptide requires that EF-G dissociate, the very slow tripeptide reaction reflects the completion of the translocation reaction (see Fig 2B) and EF-G2 dissociation. Tripeptide formation with EF-G1 (Fig 2B) was too rapid to estimate the dissociation rate. These results demonstrate that EF-G2 is able to support translation, albeit at much slower rates than the conventional EF-G species.

We considered the possibility of the alarmone ppGpp impacting translocation by EF-G1 and/or EF-G2 because: (i) it inhibits various GTPases involved in mRNA translation and ribosome biogenesis (Rojas *et al*, 1984; Mitkevich *et al*, 2010; Corrigan *et al*, 2016; Pausch *et al*, 2018; Diez *et al*, 2020; Vinogradova *et al*, 2020); and (ii) carbon starvation triggers accumulation of both ppGpp (Schofield *et al*, 2018) and the mRNA corresponding to the EF-G2-encoding *BT2167* gene (Townsend II *et al*, 2020) in *B. thetaiotaomicron*.

 © 2022 The Authors

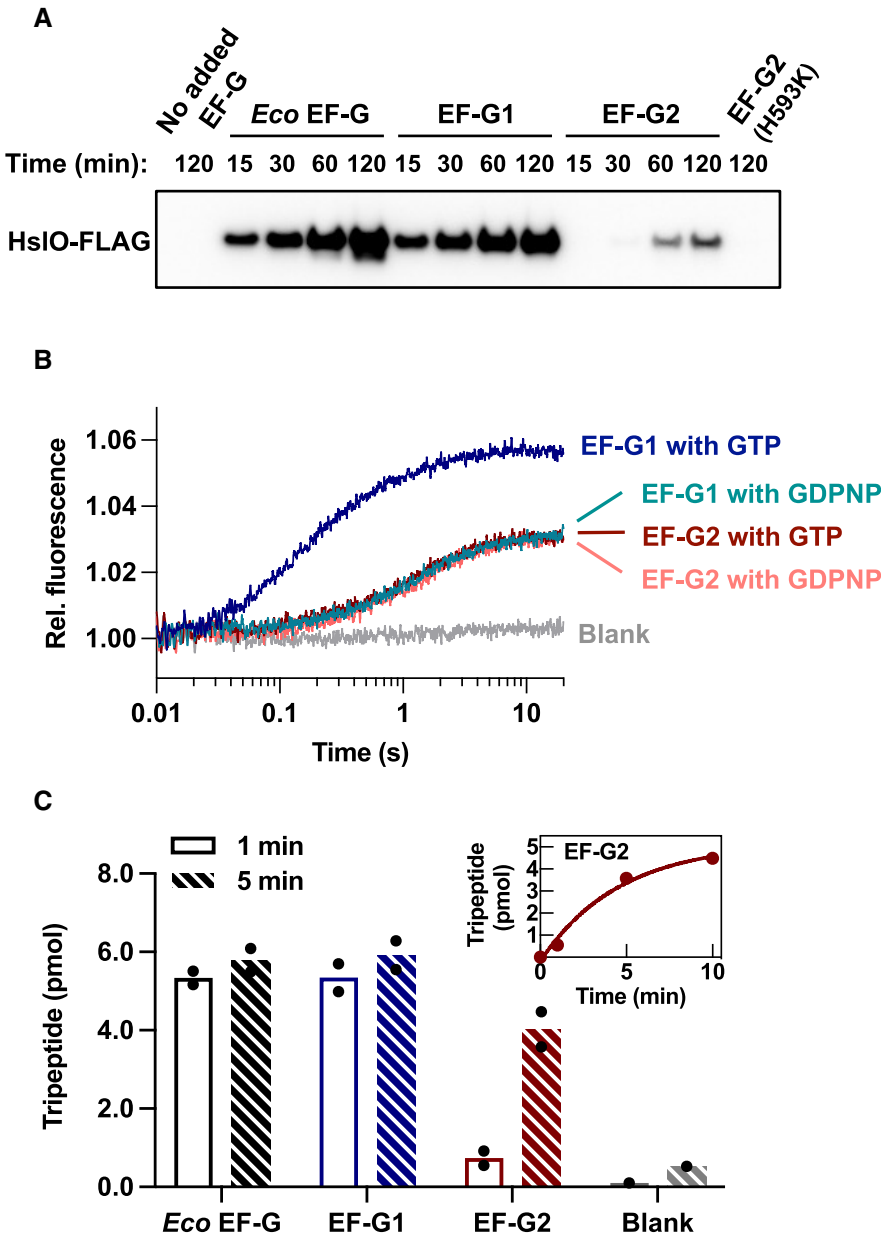

Figure 2. *B. thetaiotaomicron* EF-G2 supports slower translation elongation than *B. thetaiotaomicron* EF-G1 and *E. coli* EF-G.

A Western blot analysis of reporter HsIO-FLAG protein produced with a custom-made PURExpress® coupled *in vitro* transcription-translation system supplemented with the indicated EF-G proteins and incubated for the indicated times. Blot was developed using anti-FLAG antibodies. Shown is a representative from at least two independent experiments. *Eco* EF-G: *E. coli* EF-G.

B Ribosome translocation determined as the fluorescence change of the fluoresceine-labeled mRNA in stopped-flow experiment supplemented with the indicated proteins and nucleotides. Translocation rates are as follows: EF-G1 with GTP, 6.9 ± 0.1 s^{-1}; EF-G1 with GDPNP, 0.64 9 ± 0.01 s^{-1}; EF-G2 with GTP, 0.7 ± 0.01 s^{-1}; EF-G2 with GDPNP, 0.62 ± 0.01 s^{-1}. See Materials and Methods for details. Shown are averages of 5–7 technical replicates.

C Tripeptide formation assay using translation initiation complex programed with the tripeptide-encoding mRNA, corresponding aminoacyl-tRNA:EF-Tu:GTP ternary complexes and GTP, and the indicated EF-G proteins following incubation for 1 or 5 min. Shown are the results from two independent experiments and their average. Insert: tripeptide formation with EF-G2 following incubation for 0, 1, 5, and 10 min.

However, ppGpp failed to inhibit translocation by either EF-G1 or EF-G2 when present at equimolar amounts as GTP (Fig EV2B).

In agreement with the results of the *in vitro* protein synthesis experiments discussed above, both EF-G1 and EF-G2 co-sedimented with translating polysomes when a *B. thetaiotaomicron* cell lysate was applied to a sucrose gradient and subjected to centrifugation (Fig EV2C), indicating that both EF-G1 and EF-G2 interact with translating ribosomes *in vivo*.

We next examined if EF-G2 functions during ribosome recycling. When incubated with IF3 and monitored ribosomal complex

© 2022 The Authors

disassembly by light scattering, *B. thetaiotaomicron* EF-G1 and *B. thetaiotaomicron* RRF promoted splitting of vacant *E. coli* 70S ribosomes, although the effect was small when compared to reactions catalyzed by *E. coli* EF-G and *E. coli* RRF (Fig EV2D). By contrast, no ribosome splitting was observed with *B. thetaiotaomicron* EF-G2 and *B. thetaiotaomicron* RRF, which appeared to stabilize the ribosomal complex (Fig EV2D).

Cumulatively, the results in this section establish that EF-G2 is a *bona fide* translation elongation factor that mediates translocation, albeit at a slower rate than canonical EF-G proteins. Moreover, they raised the possibility that EF-G2 lacks the ability to bind or hydrolyze GTP.

EF-G2 lacks ribosome-stimulated GTPase activity

Canonical EF-G hydrolyses GTP in the presence of vacant or pre-translocation ribosomes (Rodnina *et al*, 1997). The *B. thetaiotaomicron* EF-G1 exhibited similar GTPase activity to *E. coli* EF-G (Figs 3A and EV3A). By contrast, EF-G2 did not hydrolyze GTP in the presence of vacant *E. coli* ribosomes (Fig EV3A) or crude ribosomes purified from *B. thetaiotaomicron* (Fig 3B). EF-G2 also lacked GTPase activity in the presence of pre-translocation *E. coli* ribosomes (Fig 3A), indicating that it does not hydrolyze GTP when mediating translocation. Control experiments demonstrated that, like *E. coli* EF-G (Kuriki *et al*, 1970), neither EF-G1 nor EF-G2 display intrinsic GTPase activity (Fig EV3B).

EF-G2 inhibited ribosome-stimulated GTP hydrolysis by EF-G1 (Fig 3C), suggesting that EF-G2 and EF-G1 bind to the ribosome at overlapping sites. However, EF-G2 appears to have lower affinity for the ribosome than EF-G1 because ~2.5 times more EF-G2 than EF-G1 was necessary to reduce EF-G1-stimulated GTP hydrolysis by half (Fig 3C).

Using differential radial capillary action of ligand assay (DraCALA; Roelofs *et al*, 2011), we determined that EF-G2 binds GTP with higher affinity than EF-G1 (Figs 3D and EV3C).

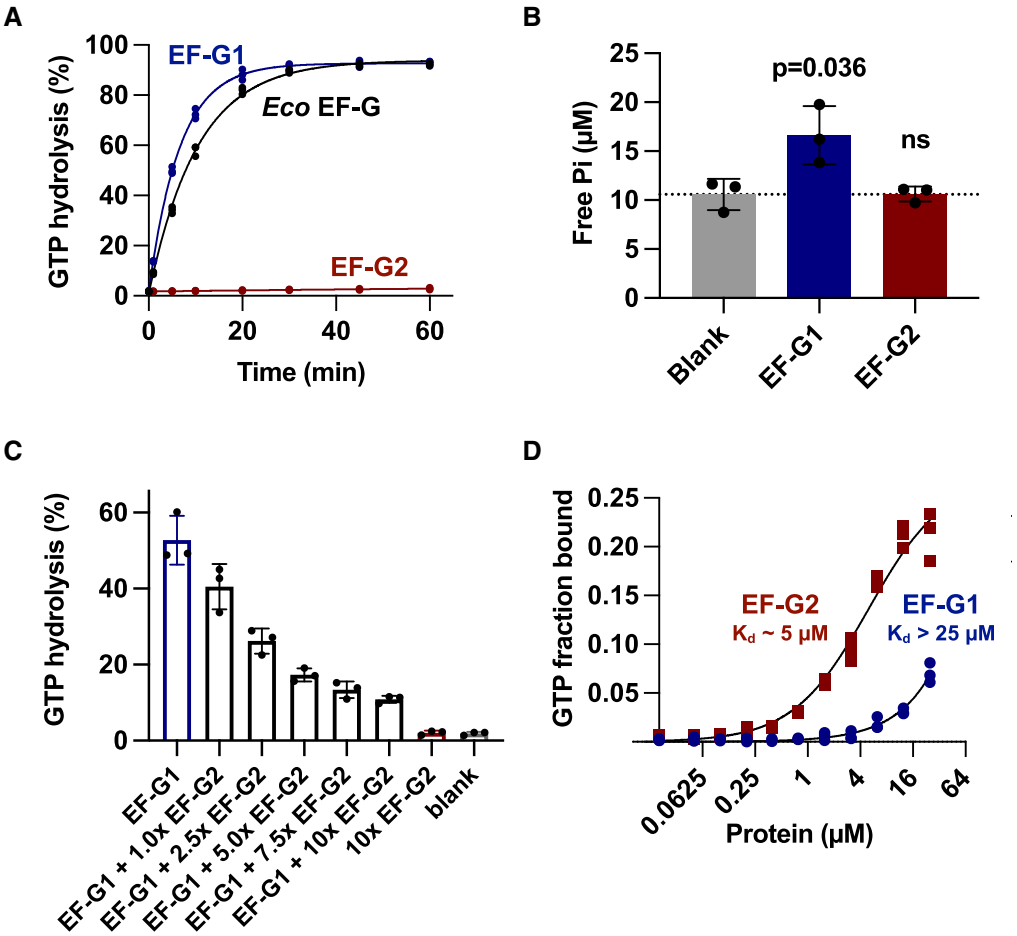

Figure 3. EF-G2 binds GTP but lacks ribosome-stimulated GTPase activity.

A GTP hydrolysis exhibited by the indicated EF-G proteins in the presence of pre-translocation ribosomes. Shown are the results from three independent experiments.

B GTP hydrolysis exhibited by the indicated EF-G proteins in the presence of a *B. thetaiotaomicron* ribosome preparation. Shown are the results from three technical replicates and their average, error bars correspond to SD. *P*-values are from two-tailed Student's *t*-test between each protein and the blank, ns indicate $P > 0.05$.

C GTP hydrolysis by EF-G1 (1 μM) measured in the presence of a fixed amount of vacant *E. coli* ribosomes and varied amounts of EF-G2 (1–10 μM, 1×–10×). Shown are the results from three independent experiments and their average, error bars correspond to SD.

D GTP binding by EF-G1 and EF-G2 measured using differential radial capillary action of ligand assay (DraCALA; Roelofs *et al*, 2011). Shown are results of three technical replicates. The DraCALA blot of one representative replicate is shown in Fig EV3C. See Materials and Methods for details.

 © 2022 The Authors

Additionally, unlabeled GTP was better than GDP at competing with radiolabeled GTP for binding to EF-G2 (Fig EV3D), suggesting that EF-G2 has higher affinity for GTP than for GDP.

These results demonstrate that EF-G2 lacks ribosome-stimulated GTPase activity, despite binding GTP and the ribosome. To our knowledge, EF-G2 is the first example of an EF-G protein that sustains translation elongation despite lacking ribosome-stimulated GTPase activity.

An EF-G2-specific region required for protein synthesis

A salient property of the EF-G2 subfamily of proteins is the presence of insertions and deletions, which is uncommon in other EF-G subfamilies (Margus *et al*, 2011). The *B. thetaiotaomicron* EF-G2 protein harbors a 26-amino acid long insert (positions 514 to 539; Figs 4A and EV1A; Margus *et al*, 2011) that is absent from translocation-competent EF-G proteins, such as *E. coli* EF-G, *T. thermophilus* EF-G, and *T. thermophilus* EF-G2 (Connell *et al*, 2007). An EF-G2 variant lacking the insert is unable to sustain protein synthesis (Fig 4B) even though it exhibits low ribosome-stimulated GTPase activity, unlike wild-type EF-G2, albeit much lower than that exhibited by EF-G1 (Fig 4C).

In the cryo-EM structure (discussed in detail in the following section), the insert is resolved as a protrusion consisting of a beta-hairpin and an additional beta-strand on the beta-sheet of domain IV of EF-G2 (Fig 4A). A comparison of the insert-less variant EF-G2 (Δ514–539) to the variant EF-G2 (Δ516–527) lacking only the beta-hairpin revealed distinct biochemical properties. While both EF-G2 variants failed to sustain protein synthesis (Fig 4B), the EF-G2 (Δ516–527) variant had no ribosome-stimulated GTPase activity (Fig 4C), like to the wild-type EF-G2 protein, whereas the EF-G2 (Δ514–539) variant had some low GTPase activity (Fig 4C). Notably, inserts are shorter in EF-G2 proteins from *Bacteroidetes* outside the *Bacteroidia* class (the one to which *Bacteroides* species belong), lacking most of the hairpin region (Fig EV1B).

We next asked if the insert is required for EF-G2 to dissociate from the ribosome. This property enables the naturally GTPase-deficient EF-G2 to continue protein synthesis (Fig 2A and C), which sets it apart from the GTPase-deficient variant of *E. coli* EF-G with the H91A substitution (Cunha *et al*, 2013). We determined that large amounts of the EF-G2 (Δ516–527) and EF-G2 (Δ514–539) variants co-sedimented with ribosomes when incubated with GTP, centrifuged on a sucrose cushion, and analyzed in the pelleted ribosomal complex by SDS–PAGE (Fig 4D). These EF-G2 variants were recovered at near stoichiometric amounts with the ribosomal proteins, indicating that they form a stable complex with the ribosome. By contrast, little wild-type EF-G2 or EF-G1 was detected in the pellet fraction with ribosomal proteins (Fig 4D).

We explored the possibility that EF-G2 lacks GTPase activity due to the presence of a serine instead of histidine at position 84 (corresponding to H91 in *E. coli* EF-G). However, the EF-G2 (S84H) variant exhibited marginally higher GTPase activity than wild-type EF-G2 (Fig 4C) that is not statistically significant ($P = 0.12$ two-tailed Student's *t*-test). Curiously, the EF-G2 (S84H) variant supported faster protein synthesis than wild-type EF-G2 (Fig 4E).

Collectively, the results in this section identify a region of EF-G2 necessary for protein synthesis despite being absent from other EF-G proteins, including members of the EF-G2 subfamily. In addition, they indicate that the identified region contributes to both the lack of GTPase activity and to EF-G2's dissociation from the ribosome.

Ribosome-bound EF-G2 in the GTP-bound conformation reveals GTPase domain shifted away from the sarcin-ricin loop

To gain insights into EF-G2's unique biochemical properties, we examined the structure of EF-G2 bound to the *E. coli* ribosome using cryo-EM (see Materials and Methods for details about the cryo-EM data collection and structure solving). From a sample containing ribosomes, EF-G2, and GTP in a buffer with 10 mM Mg^{2+}, we obtained density maps for vacant ribosomes (70S) and ribosome-EF-G2 complexes (70S-EF-G2; Appendix Fig S1) at a global resolution of 2.7 and 2.9 Å, respectively (Appendix Fig S2A and B). After 3D classification, the two best classes of 70S-EF-G2 particles (Class 1 and Class 2) were further refined to a global resolution of 3.2 and 3.0 Å, respectively (Appendix Figs S1, and S2C and D). Class 1 corresponds to EF-G2 bound to a non-rotated ribosome with ~2° of 30S head domain swiveling (Fig EV4A). Class 2 corresponds to EF-G2 bound to the ribosome with ~4° of inter-subunit rotation and ~16° of 30S head swiveling (Fig EV4A).

Our analysis revealed that EF-G2 binds the ribosome at the same site used by the canonical EF-G protein (Fig 5A). The overall five-domain structure of *E. coli* EF-G is preserved in EF-G2 (Fig 5B and C), except for the 26-amino acid insert in domain IV of EF-G2 forming a protrusion consisting of a beta-hairpin and an additional beta-strand on the domain IV beta-sheet (Fig 5D). On the non-rotated ribosome (Class 1), the insert is near the 30S head (Fig EV4B), being closest to the C-terminus of ribosomal protein S19, helix 31, and ~U1502 of 16S rRNA. (Please note that the resolution in this region is ~6–7 Å due to the dynamic nature of 30S head domain.)

Figure 4. Biochemical features of *B. thetaiotaomicron* EF-G2.

A Structure of EF-G2 domain IV highlighting the insert (residues 514–539) and hairpin (residues 516–527) regions.

B Western blot analysis of reporter HslO-FLAG protein synthesized *in vitro* using a custom-made PURExpress® system with EF-G1, EF-G2, and two engineered EF-G2 variants: one missing the 26-amino acid insert, EF-G2 (Δ514–539) and one missing the beta hairpin in the insert, EF-G2 (Δ516–527). Shown is a representative experiment from at least two independent experiments.

C GTP hydrolysis by EF-G1, EF-G2 and indicated variants incubated in the presence of vacant *E. coli* ribosomes. Shown are results from three technical replicates and their average, error bars correspond to SD, and *P*-values derived from two-tailed Student's *t*-test comparing each protein to the blank.

D SDS–PAGE analysis of co-sedimentation assays monitoring factor (EF-G1 EF-G2 or EF-G2 variant EF-G2 (Δ516–527) or EF-G2 (Δ514–539)) binding to *E. coli* 70 S ribosomes. Binding reactions were centrifuged through a sucrose cushion to recover ribosome and associated factor in the pellets. The positions of EF-G proteins and ribosomal proteins and molecular weight markers are indicated.

E Western blot analysis of reporter HisC-FLAG protein synthesized *in vitro* using a custom-made PURExpress® system with the EF-G1, EF-G2 or EF-G2 (S84H) proteins. Shown is a representative from at least two independent experiments.

© 2022 The Authors

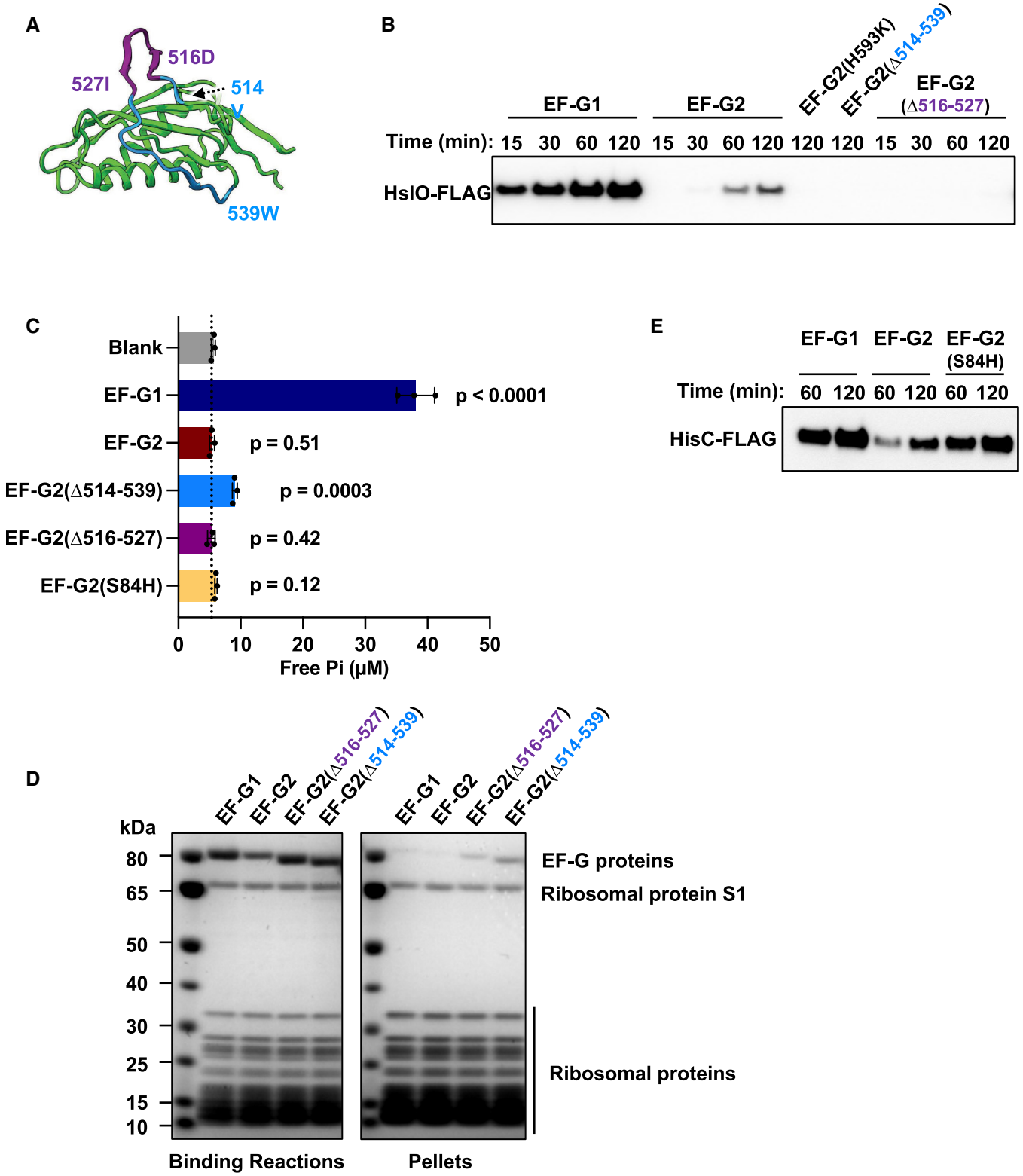

Figure 4.

Ligand density consistent with a GTP can be seen in the GTP-binding pocket of domain I in EF-G2 (Fig 5E and F), with local resolution around 3.7 Å (Appendix Fig S2F). The EF-G2 switch I and switch II regions are fully resolved and structured like those of canonical EF-G and *T. thermophilus* EF-G2 in their active (GTP/GDP-Pi/GTP-analog binding) forms (Fig 5G; Connell *et al*, 2007; Pulk & Cate, 2013; Tourigny *et al*, 2013; Zhou *et al*, 2013; Carbone *et al*, 2021; Petrychenko *et al*, 2021; Rundlet *et al*, 2021).

 © 2022 The Authors

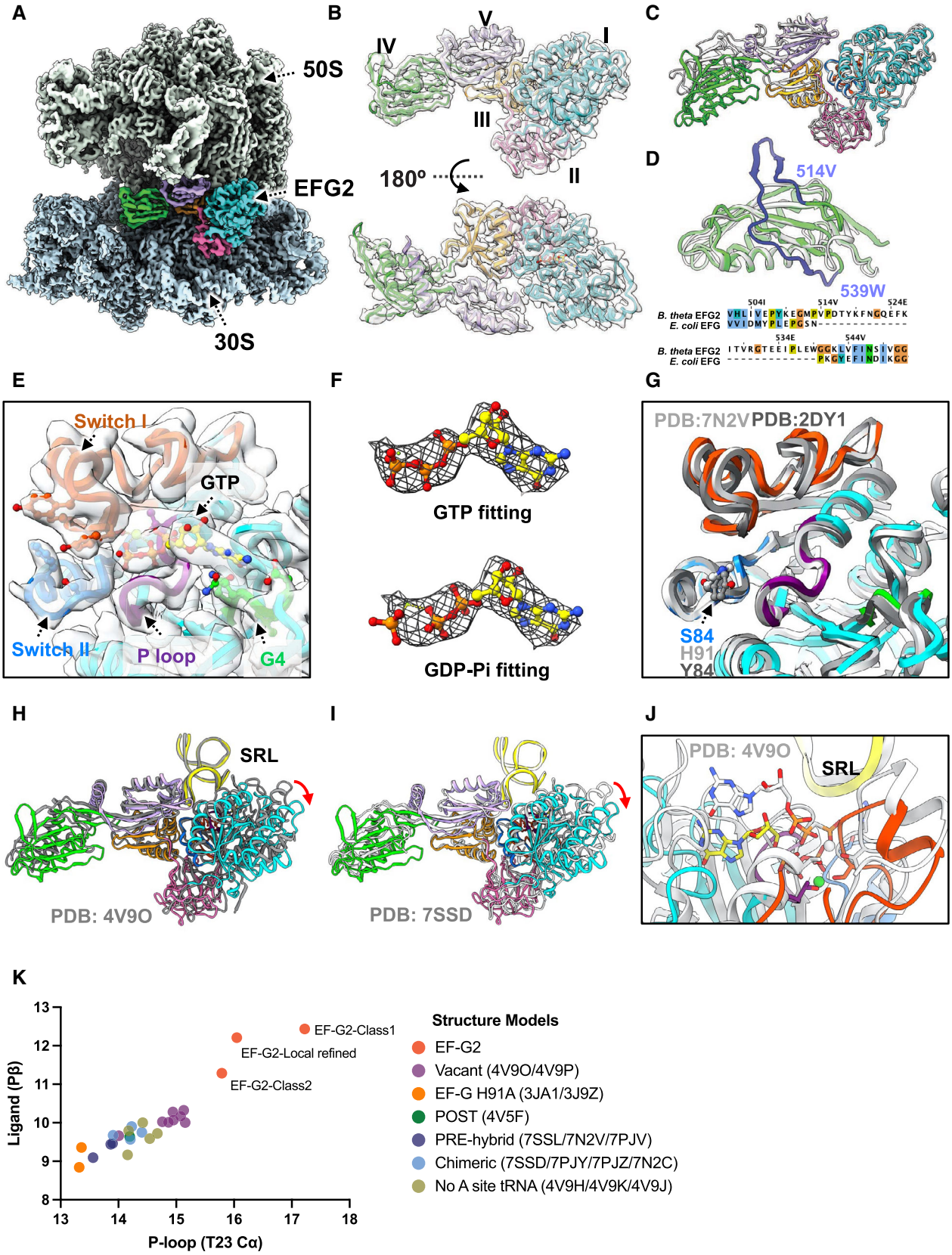
A
50S
EFG2
30S
B
V
IV
I
III
180º
II
C
D
514V
539W
B. theta EFG2
E. coli EFG
E
Switch I
GTP
Switch II
P loop
G4
F
GTP fitting
GDP-Pi fitting
G
PDB:7N2V
PDB:2DY1
S84
H91
Y84
H
SRL
PDB: 4V9O
I
PDB: 7SSD
J
PDB: 4V9O
SRL
K
Ligand (Pβ)
P-loop (T23 Cα)
EF-G2-Class1
EF-G2-Local refined
EF-G2-Class2
Structure Models
EF-G2
Vacant (4V9O/4V9P)
EF-G H91A (3JA1/3J9Z)
POST (4V5F)
PRE-hybrid (7SSL/7N2V/7PJV)
Chimeric (7SSD/7PJY/7PJZ/7N2C)
No A site tRNA (4V9H/4V9K/4V9J)

Figure 5.

Figure 5. Structure of the EF-G2-ribosome complex revealed by Cryo-EM.

A Overview of the EF-G2-ribosome complex structure. The ribosomal 50S subunit is in gray and the 30S subunit in light blue. The color of the five domains of EF-G2 are as follows: blue—I, pink—II, orange—III, green—IV, light purple—V. The same color scheme for the EF-G2 domains is used in other panels.

B Overview of the five-domain structure of the EF-G2 protein.

C Comparison of the EF-G2 structure with that of *E. coli* EF-G (PDB: 7N2V) in light gray. The structures are aligned by their domain I.

D Comparison of domain IV of EF-G2 and *E. coli* EF-G (PDB: 7N2V) in light gray, highlighting the 26-amino acid insert present in EF-G2 (residues 514–539) and absent from EF-G1 and *E. coli* EF-G (Fig EV1).

E Local density and model fitting of the resolved switch I and II regions and GTP in the ligand-binding pocket of EF-G2. The switch I (residues K37-L67) region is colored orange, the switch II (D80-V97) region blue, the P-loop (G16-T23) purple and the G4-box (N134-D137) region green. The same color scheme is used in other panels for EF-G2.

F Fitting GTP or GDP-Pi in the density of the ligand showing GTP fits better. The models of *T. thermophilus* EF-G2-GTP (PDB: 2DY1) or *E. coli* EF-G-GDP-Pi (PDB: 7SSL) were rigid-body fitted in focused refined EF-G2 map, and density corresponding to the ligand were extracted as shown in the upper and lower panels, respectively.

G Superimposed structures of the GTP-binding pocket including the switch I and II regions of EF-G2 and the GTP-bound conformation of *E. coli* EF-G (PDB: 7N2V, light gray) and *T. thermophilus* EF-G2 (PDB: 2DY1, dark gray).

H, I Superimposed structures showing position of the ribosomal sarcin-ricin loop (SRL, yellow) relative to EF-G2 (colored) or GDPCP-bound *E. coli* EF-G on vacant ribosome (PDB: 4V9O) (dark gray) (H), and GDP-bound *E. coli* EF-G on chimeric translocation intermediate (PDB: 7SSD) (light gray) (I). Structures were aligned by the 23S rRNA. Red arrows indicate the rotation of EF-G2 domains I and II relative to *E. coli* EF-G structures. Same color scheme for EF-G2 as in previous panels.

J Superimposed structures showing position of the SRL (yellow) relative to the GTP binding pocket of EF-G2 (colored) or GDPCP-bound *E. coli* EF-G on vacant ribosome (PDB: 4V9O) (light gray).

K Distance (in Å) between SRL (Cα of A2662) and GTP-binding pocket (Cα of T23 in the P-loop and Pβ of the ligand GTP/analog/GDP/GDP-Pi) in the EF-G2 structures and in published structures of ribosome-bound *E. coli* or *T. thermophilus* EF-G with PDB identifiers indicated in parenthesis.

In the complex with the ribosome, domains I and II of EF-G2 shift away from the sarcin-ricin loop (SRL) of the 23S rRNA, adopting an orientation not previously observed in ribosomes complexed with canonical EF-G proteins (Fig 5H and I; Gao *et al*, 2009; Pulk & Cate, 2013; Tourigny *et al*, 2013; Zhou *et al*, 2013; Carbone *et al*, 2021; Petrychenko *et al*, 2021; Rundlet *et al*, 2021). Meanwhile, the distance between the GTP-binding pocket of EF-G2 and the SRL in the 70S-EF-G2 complexes (local resolution ~3.7 Å, 11.3–12.4 Å between Cα of A2662 and Pβ of the ligand) is much longer than that in previously reported structures of canonical EF-G-ribosome complexes (8.8–10.3 Å between Cα of A2662 and Pβ of the ligand; Fig 5J and K), in which the SRL is closely packed with the GTP-binding pocket and essential for GTPase activation and EF-G binding (Clementi *et al*, 2010; Voorhees *et al*, 2010; Shi *et al*, 2012; Petrychenko *et al*, 2021). The GTP-binding pocket is closely packed with the SRL even in the structures of the GTPase-defective *E. coli* EF-G (H91A) bound to the ribosome (Fig 5K; Li *et al*, 2015). As the release of the *E. coli* EF-G domain I from the SRL initiates the dissociation of the factor from the ribosome (Carbone *et al*, 2021), the longer separation of EF-G2 from the SRL may facilitate EF-G2 clearance of the ribosome, thereby enabling turnover translation.

Domains III, IV, and V of EF-G2 adopt an orientation and position similar to the corresponding domains of *E. coli* EF-G (in the GTP-analog-bound form) on ribosomes without mRNA and tRNA (Fig 5H; Pulk & Cate, 2013), on ribosomal complexes without A-site tRNA (Tourigny *et al*, 2013; Zhou *et al*, 2013), in GDP-bound form on a post-translocation ribosome (Gao *et al*, 2009), or in GDP-bound form on translocation intermediates (Fig 5I) in which the peptidyl-tRNA has moved to the ap/P state, vacating the A site on the 30S body domain (Carbone *et al*, 2021; Petrychenko *et al*, 2021; Rundlet *et al*, 2021), with domain IV of EF-G2 reaching into the A site of the 30S body. The ap/P (also called chimeric) state is a bona-fide intermediate of translocation, suggesting that EF-G2 promotes tRNA–mRNA movement along a similar trajectory.

Cumulatively, this analysis revealed EF-G2 in GTP-bound conformation interacting with the ribosome but not in close contact with the SRL, a critical element of the GTPase center formed by translational GTPases and the ribosome.

EF-G2 is expressed under starvation conditions and is the dominant EF-G protein in *B. thetaiotaomicron* harvested from the murine gut

To understand the role of EF-G2 in *B. thetaiotaomicron*'s lifestyle, we compared its abundance to that of EF-G1 in strains expressing epitope-tagged versions of these proteins from their normal promoters and chromosomal locations. Western blot analysis of bacterial crude extracts revealed that EF-G2 abundance is exceedingly low during exponential growth in complex medium but increases dramatically upon entry into stationary phase (Fig 6B–D). EF-G2 also accumulated upon carbon starvation (Fig EV5B and C), reflecting the increase in the corresponding mRNA (Townsend II *et al*, 2020), but not in response to nitrogen starvation (Fig EV5B and C). By contrast, EF-G1 is highly abundant during all phases of growth in complex medium, reaching its peak values during early exponential phase and gradually decreasing as the culture reaches stationary phase (Fig 6A, C and D). EF-G1 abundance was also high in bacteria grown in minimal medium or upon a shift to carbon- or nitrogen-starvation conditions, without a significant decrease within 60 min of carbon- or nitrogen-starvation (Fig EV5A and C). In sum, EF-G1 is highly abundant under all examined laboratory conditions, whereas EF-G2 is not expressed under fast-growing conditions and accumulates upon carbon starvation.

We next investigated the abundance of EF-G1 and EF-G2 in wild-type *B. thetaiotaomicron* harvested from the ceca of mono-colonized mice 4 days after oral gavage, using antisera raised against recombinant EF-G1 and EF-G2 proteins, which showed excellent specificity to their corresponding antigens and little cross-reactivity (Appendix Fig S3). First, EF-G1 was barely detected in bacteria harvested from the cecum (Fig 6E), which was unexpected given that EF-G1 amounts are higher in bacteria grown in laboratory media (Fig 6A) and that the *BT2729* gene encoding EF-G1 is essential (Goodman *et al*, 2009). Second, EF-G2 amounts were as high in bacteria harvested from the cecum (Fig 6E) as in bacteria from stationary phase laboratory cultures (Fig 6E and F). By normalizing the signals from bacteria harvested from mice to those of known amounts of purified EF-G1 and EF-G2, we estimate that EF-G2

 © 2022 The Authors

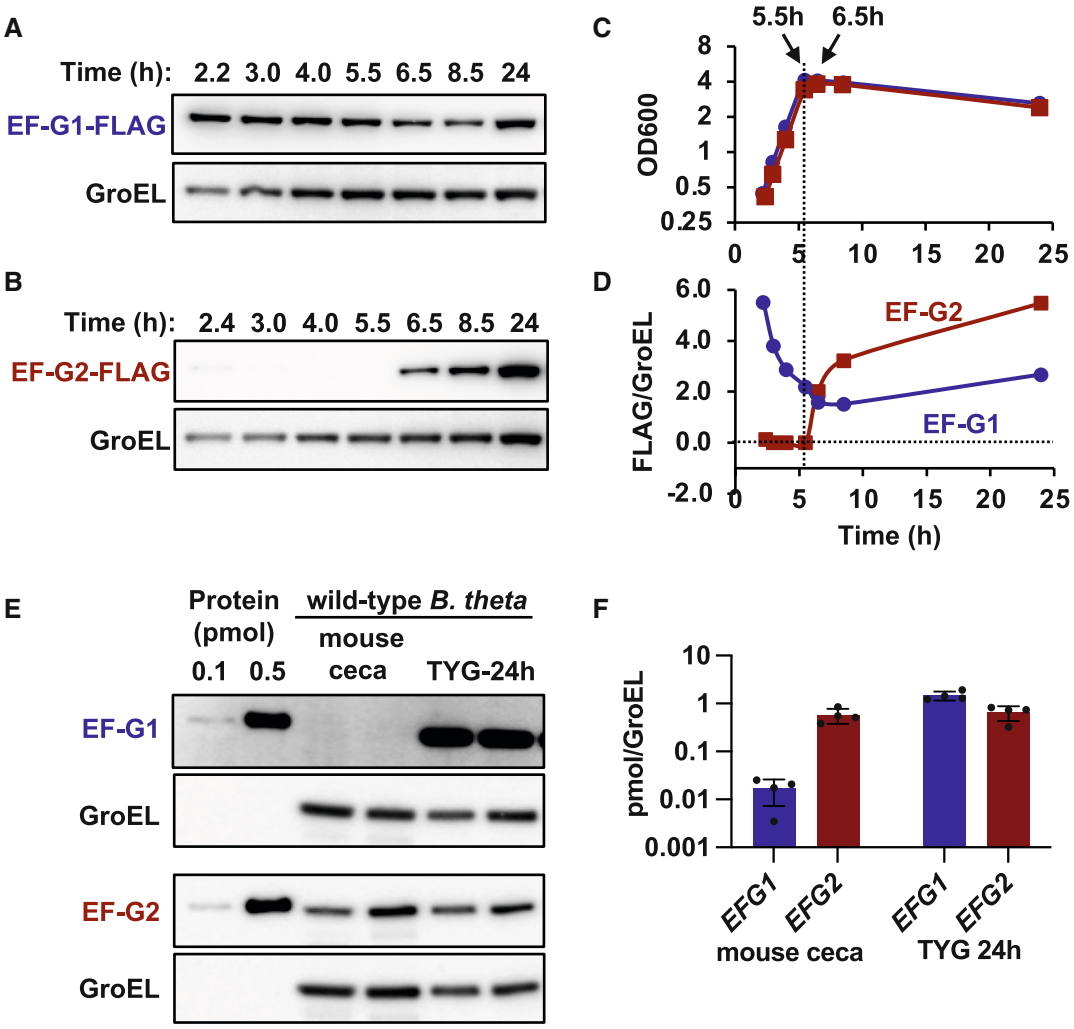

Figure 6. Differential expression of the EF-G1 and EF-G2 protein in laboratory medium and mouse cecum.

A–D Western blot analysis of *B. thetaiotaomicron* strains expressing C-terminally FLAG-tagged EF-G1 (WH405) (A), or EF-G2 (GT1301) (B), from their normal promoters and chromosomal locations, grown in Tryptone Yeast Extract Glucose liquid medium (TYG) and sampled at the indicated times. Bacterial growth (OD_{600}) is shown in (C) and Western blot quantifications (FLAG signal normalized to loading control GroEL) are show in (D). Blots were developed with anti-FLAG antibodies; anti-GroEL antibodies were used as loading controls. Shown is a representative from at least two independent experiments.

E, F Western blot of crude extracts from wild-type *B. thetaiotaomicron* harvested from the ceca of mice (representative blot for two out of four mice tested) or corresponding to stationary phase cultures harvested following growth in TYG for 24 h or purified EF-G1 and EF-G2 proteins at the indicated amounts (E). Blots were developed with anti-EF-G1 or EF-G2 polyclonal antibodies; anti-GroEL antibodies were used as loading controls. Western blot quantifications of all four biological replicates and their average are shown in (F), where EF-G1 and EF-G2 abundances were estimated by normalizing the signal of bacterial sample to the closest signal of known amount of purified protein, and the derived absolute amount (pmol) was normalized to the signal of GroEL. Error bars represent SD. Please note log scale of *y* axis.

abundance surpasses EF-G1's by at least 10-fold in the murine gut (Fig 6F).

In sum, *B. thetaiotaomicron* increases EF-G2 amounts while decreasing the abundance of the essential EF-G1 in the murine cecum, suggesting that EF-G2-mediated protein synthesis is necessary for gut colonization.

Gut colonization by *B. thetaiotaomicron* requires EF-G2's ability to support translation elongation

An EF-G2 null mutant is defective in murine gut fitness (Townsend II *et al*, 2020). This defect appears to be largely due to EF-G2's role in protein synthesis because a *B. thetaiotaomicron* strain harboring the EF-G2 (H593K) variant inactive in protein synthesis (Fig 2A) was as defective for gut colonization as an isogenic EF-G2 null mutant (Fig 7): when the four isogenic *B. thetaiotaomicron* strains were inoculated in germ-free mice at nearly identical amounts, the *BT2167* null mutant (lacking EF-G2) and the *BT2167* null mutant complemented *in trans* with a mutant *BT2167* gene specifying the variant EF-G2 (H593K) were out-competed by wild-type *B. thetaiotaomicron* and the isogenic *BT2167* null mutant complemented with the wild-type *BT2167* gene after 1 week of colonization (Fig 7). This result argues that EF-G2's role in translocation is required for *B. thetaiotaomicron* fitness in the murine gut.

© 2022 The Authors

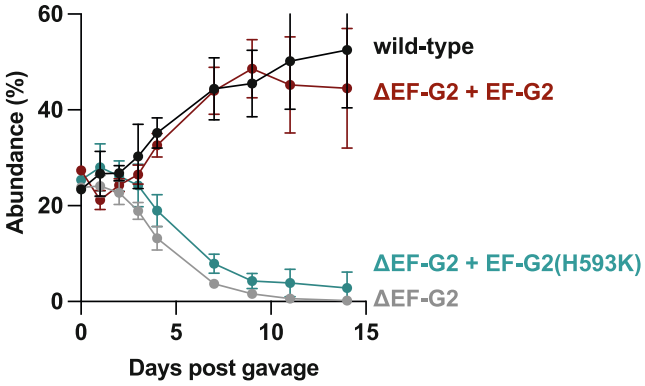

Figure 7. EF-G2-mediated protein synthesis is required for murine gut colonization.

Abundances of barcoded wild-type (GT478) and three isogenic *B. thetaiotaomicron* strains: one lacking the EF-G2-specifying gene *BT2167* (ΔEF-G2, WH148), one lacking *BT2167* and expressing the wild-type *BT2167* gene *in trans* (ΔEF-G2 + EFG2, WH160), and one lacking *BT2167* and expressing a variant of *BT2167* specifying an EF-G2 with the H593K substitution (ΔEF-G2 + EFG2 (H593K), WH514) in gnotobiotic mice ($N = 5$) at the indicated times following gavage. Values for day 0 are calculated using the number of colony-forming units (CFU) in the inoculum, and for day 1–14 are based on qPCR measurement of each barcode in mouse fecal sample. See Materials and Methods for details. Mean values and SD of five biological replicates are shown.

Discussion

In all kingdoms of life, protein synthesis requires an essential GTPase to promote ribosome translocation. Designated EF-G in *E. coli*, this canonical GTPase hydrolyzes GTP on the ribosome, accelerating ribosome translocation by four orders of magnitude during protein synthesis (Noller *et al*, 2017; Rodnina *et al*, 2019). We have now identified a natural paralog of this GTPase that promotes slow ribosome translocation and supports slow protein synthesis (Fig 2) without hydrolyzing GTP (Figs 2B and 3). Designated EF-G2 in *B. thetaiotaomicron*, this protein binds GTP (Figs 3D and 5E) but lacks the ribosome-stimulated GTPase activity (Figs 3A and EV3A) of canonical EF-G proteins (Rodnina *et al*, 1997).

Specifically induced under carbon starvation laboratory conditions (Figs 6B and EV5B; Townsend II *et al*, 2020), EF-G2 enables the prominent commensal *B. thetaiotaomicron* to colonize the mammalian gut by supporting essential protein synthesis (Figs 2A and 7) in a slow but energy-saving manner (Fig 3A). *B. thetaiotaomicron* also harbors EF-G1, an ortholog of *E. coli* EF-G that is highly abundant under all tested laboratory conditions (Figs 6A and EV5A) but largely reduced in the murine gut, being surpassed by EF-G2 by > 10-fold (Fig 6F). These findings suggest that paralogous EF-Gs enable *B. thetaiotaomicron* to switch between rapid and energy-efficient modes of protein synthesis in nutrient-fluctuating environments.

EF-G2 supports translation elongation without hydrolyzing GTP

GTP-hydrolysis by canonical EF-G accelerates ribosome translocation and allows the GDP-bound form to dissociate from the ribosome (Inoue-Yokosawa *et al*, 1974; Belitsina *et al*, 1975, 1976; Kaziro, 1978; Rodnina *et al*, 1997; Cunha *et al*, 2013; Belardinelli *et al*, 2016). When GTP hydrolysis is blocked (e.g., by a non-hydrolysable GTP analog or mutation of a catalytic His91 residue in the protein), EF-G is trapped on the ribosome following a single round of slow ribosome translocation (Inoue-Yokosawa *et al*, 1974; Cunha *et al*, 2013; Salsi *et al*, 2016), thereby blocking subsequent binding of aminoacyl-tRNA.

Naturally lacking GTPase activity (Figs 3A and EV3A), *B. thetaiotaomicron* EF-G2 promotes slower ribosome translocation than canonical EF-G proteins (Figs 2B and EV2A), with kinetics similar to translocation mediated by EF-G1 with a non-hydrolysable GTP-analog (Fig 2B), reminiscent of the GTPase-deficient *E. coli* EF-G (H91A) variant (Cunha *et al*, 2013; Holtkamp *et al*, 2014). However, unlike the latter variant, EF-G2 dissociates spontaneously from the ribosome after promoting translocation, allowing protein synthesis to continue (Fig 2A and C). The ability of EF-G2 to dissociate from the ribosome appears to require the 26-amino acid insert in domain IV (Fig 4D), which is exclusively found in *Bacteroidia* (Figs 1A and EV1B; Margus *et al*, 2011). EF-G2 proteins from bacteria outside the *Bacteroidetes* phylum lack this insert, while EF-G2 proteins from *Bacteroidetes* outside the *Bacteroidia* class have shorter (17-amino acid) inserts lacking the hairpin region critical for EF-G2 dissociation (Fig 4). Therefore, the property of mediating turnover translocation without GTP hydrolysis is probably limited to EF-G2 members of the *Bacteroides* genus and their close relatives.

We propose that EF-G2 binds the ribosome and promotes translocation when bound to GTP because: (i) EF-G2 binds GTP with a micromolar affinity (Fig 3D) and has a higher affinity for GTP than GDP (Fig EV3D). Thus, EF-G2 should be in GTP-bound form in cells because the cellular GTP concentration is at millimolar level and usually higher than the GDP concentration. (Please note that the GTP/GDP ratio does not change significantly before or after 1 h of carbon starvation in *B. thetaiotaomicron* (Schofield *et al*, 2018).) (ii) Density of a ligand consistent with GTP is visualized in the cryo-EM structure of EF-G2 bound to the ribosome (Fig 5E and F). (iii) There are similarities between the structure of EF-G2 when bound to the vacant ribosome and that of the canonical EF-G bound to ribosomes without tRNA or mRNA or to ribosome complexes in the intermediate state of translocation (Fig 5H and I). Therefore, the EF-G2 structure resembles those of canonical EF-G proteins that promote translocation when bound to GTP, GDP-Pi, or non-hydrolysable GTP-analogs but not to GDP or in ligand-free form (Inoue-Yokosawa *et al*, 1974; Belitsina *et al*, 1975, 1976; Rodnina *et al*, 1997; Salsi *et al*, 2016).

Ribosome recycling strictly requires EF-G-dependent GTP hydrolysis and phosphate release (Savelsbergh *et al*, 2009). This contrasts with EF-G-stimulated ribosome translocation, which is still supported by EF-G in the absence of GTP hydrolysis (Inoue-Yokosawa *et al*, 1974; Rodnina *et al*, 1997; Cunha *et al*, 2013; Salsi *et al*, 2016). In agreement with this notion, both EF-G1 and EF-G2 support translocation in *E. coli* ribosomes (Fig 2), but only the GTPase-competent EF-G1 exhibited ribosome recycling activity (Fig EV2D); EF-G2 was inactive in ribosome disassembly and actually stabilized the ribosomal complex (Fig EV2D). The inability of EF-G2 to support ribosome recycling may also explain the essentiality of the EF-G1-encoding *BT2729* gene (Goodman *et al*, 2009).

 © 2022 The Authors

Colonization of the mammalian gut requires energy-efficient protein synthesis

The mammalian gut environment is rich in dietary and host-derived carbohydrates (or glycans) that provide sufficient carbon and energy to support over 10^{11} microbial cells per milliliter (Donaldson *et al*, 2016; Sender *et al*, 2016). However, systems that respond to nutrient limitation *in vitro* are critical for intestinal colonization (Schofield *et al*, 2018; Townsend II *et al*, 2020), indicating that microbes experience nutrient limitation in the gut, likely due to fluctuations in available nutrients and competition with other gut residents. The prevalent commensal *B. thetaiotaomicron* requires the alarmone (p)ppGpp to colonize the gut and produces (p)ppGpp in response to carbon starvation (Schofield *et al*, 2018) rather than amino acid limitation, as enteric bacteria do (Cashel & Gallant, 1969; Haseltine *et al*, 1972). Moreover, carbon starvation activates transcription factor BT4338, a master regulator of carbohydrate utilization and gut colonization (Wu *et al*, 2015; Schwalm III *et al*, 2016; Townsend II *et al*, 2020), which activates transcription of the EF-G2-specifying *BT2167* gene > 100-fold and of genes involved in energy generation (Townsend II *et al*, 2020).

EF-G2 appears to be largely responsible for protein synthesis some of the time *B. thetaiotaomicron* is in the mammalian gut because EF-G2 is > 10-fold more abundant than EF-G1 in bacteria recovered from the mouse cecum (Fig 6E and F) and because the ability of EF-G2 to support protein synthesis (Fig 2A) is necessary for *B. thetaiotaomicron* fitness in the gut (Fig 7). Although slower than EF-G1-mediated protein synthesis (Fig 2A), EF-G2-mediated protein synthesis confers the unique advantage of not consuming GTP at each ribosome translocation step (Figs 2C and 3A), unlike protein synthesis supported by canonical EF-G (Rodnina *et al*, 1997). That is, by employing EF-G2, *B. thetaiotaomicron* saves energy at the costliest step of protein synthesis. In addition, EF-G1, like canonical EF-G, can hydrolyze GTP non-productively when interacting with ribosomes not engaged in translation (Fig EV3A), unlike EF-Tu, the other factor involved in translation elongation, that stimulates GTP hydrolysis only when engaged in translation. That EF-G2 abundance is 10-fold higher than EF-G1's (Fig 6E and F) would also prevent unnecessary energy (GTP) consumption upon EF-G1 binding to non-translating vacant ribosomes (Fig EV3A), which may accumulate during carbon starvation (Li *et al*, 2018).

Concluding remarks

Gene duplication plays a key role in the evolution of new cellular abilities because it provides the raw material for mutation and selection as well as redundant genes with reduced functional constraints (Zhang, 2003). Thus, random mutations in one of the copies of the duplicated gene, being under relaxed purifying selection, can change the function of that gene, providing an advantage under particular environmental conditions or genetic backgrounds (Dykhuizen & Hartl, 1980; Kimura, 1983).

We have now uncovered a novel function of an ancient gene duplicate in a mammalian gut commensal. We determined that the EF-G2-specifying paralog of the essential EF-G-specifying gene encodes a starvation-induced translation factor that mediates energy-saving *slow* protein synthesis, in contrast to that mediated by the GTP-hydrolyzing ancestral EF-G1. Significantly, a single amino acid substitution in EF-G2 can improve its protein synthesis activity (Fig 4E) but has not been selected for in *B. thetaiotaomicron*, suggesting that a reduction in the energetic costs of protein synthesis is required for the organism's lifestyle. Moreover, deploying EF-G2 under starvation conditions may provide the additional benefit of preventing ribosome collision and unnecessary abortion of translation (Subramaniam *et al*, 2014; Saito *et al*, 2022) by matching translation elongation speed to the reduced aminoacyl-tRNA substrate pool present under nutrient-limited conditions.

Finally, *Bacteroides* incorporated the energy-efficient EF-G2-specifying paralog into the regulon of the master regulator of carbohydrate utilization, energy generation, and gut colonization that is activated in response to carbon starvation (Townsend II *et al*, 2020). This evolutionary event enables bacteria to calibrate both metabolism and protein synthesis to the availability of nutrient and energy resources in the gut.

Materials and Methods

Reagents and resources

Details about key reagent, resources, software, and tools used in this work are provided in Appendix Table S1.

Bacterial strains and growth conditions

Bacteroides thetaiotaomicron VPI-5482 *tdk* (Koropatkin *et al*, 2008) and derived strains (Appendix Table S1) were cultured anaerobically at 37°C in liquid Tryptone Yeast Extract Glucose (TYG) medium (Holdeman *et al*, 1977), glucose minimal medium (MM) [100 mM KH_2PO_4 (pH 7.2), 15 mM NaCl, 8.5 mM $(NH_4)_2SO_4$, 0.5 μg ml^{-1} L-cysteine, 1.9 μM hematin, 200 μM L-histidine, 100 μM $MgCl_2$, 1.4 μM $FeSO_4$, 50 μM $CaCl_2$, 1 μg ml^{-1} vitamin K_3, 5 ng ml^{-1} vitamin B_{12}, plus 0.5% (wt/v) glucose] (Martens *et al*, 2008), or on Brain Heart Infusion Agar containing 5% defibrinated horse blood. When appropriate, antibiotics were added at the following final concentrations: tetracycline 2 μg ml^{-1}, erythromycin 10 μg ml^{-1}, or gentamicin 200 μg ml^{-1}. An anaerobic chamber (Coy Laboratory Products) containing 20% CO_2, 10% H_2, and 70% N_2 was used for all anaerobic microbiology procedures. *E. coli* S17-1 λ*pir* and *E. coli* BL21(DE3) were cultured at 37°C in Luria Bertani broth (BD), containing 100 μg ml^{-1} ampicillin when appropriate.

Gnotobiotic animal experiments

All experiments using mice were performed using protocols approved by the Yale University Institutional Animal Care and Use Committee. Germ-free C57BL/6J mice were maintained in flexible plastic gnotobiotic isolators with a 12-h light/dark cycle. Individually caged animals (N = 5 per group, littermates of mixed sex were randomly assigned to experimental groups) were fed a standard, autoclaved mouse chow (5 K67 LabDiet, Purina) *ad libitum*. Mice were 12–16 weeks of age at the time of gavage. Within a given experiment, mice were age-matched within 2 weeks.

© 2022 The Authors

Construction of strains and plasmids

Genetic engineering methods

DNA purification, PCR, and cloning were performed using standard methods. All strains and plasmids (listed in Appendix Table S1) were constructed using oligonucleotides with sequences provided in Appendix Table S2. All *B. thetaiotaomicron* strains were derived from strain VPI-5482 *tdk* (Koropatkin *et al*, 2008). Introduction of plasmid into *B. thetaiotaomicron* was achieved by conjugation with *E. coli* S17-1 λ*pir* harboring the corresponding plasmids. All plasmids were verified by Sanger sequencing across the insert before their introduction into *B. thetaiotaomicron*. Plasmids derived from pNBU2-*tetQ* and oligonucleotide barcodes encoded pNBU2-*tetQ* vectors were introduced into the *B. thetaiotaomicron* genome (NBU2 *att-1* site) in single copy as described (Martens *et al*, 2008). Introduction of the pKNOCK-*tetQ* suicide vector into *B. thetaiotaomicron* genome by homologous recombination was carried out as described (Raghavan *et al*, 2014). In-frame, unmarked, nonpolar deletions were generated using a counter-selectable allelic exchange procedure as described (Koropatkin *et al*, 2008) and confirmed by PCR and Sanger sequencing across the chromosomal region of interest.

Construction of a strain specifying BT2729 with a C-terminal tag from its native chromosomal location

We used plasmid pKNOCK-*tetQ*, cloning the 750 bp sequence at the 3′ end of the target gene including additional nucleotide sequences encoding the FLAG-tag and a stop codon as described (Townsend II *et al*, 2020), except that the *BT2731* promoter (p_{BT2731}, which transcribes the *BT2729* operon) was added in front of the 750 bp sequence, so that after plasmid integration, the genes downstream of *BT2729* were transcribed from this promoter.

Preparation of proteins and ribosomes

Protein overexpression and purification

The *BT2729*, *BT2167*, and *BT2167(H593K)* genes without the corresponding stop codons were PCR amplified using oligonucleotides with sequences provided in the Appendix Table S2 and cloned (separately) between the NdeI and XhoI sites of plasmid pET22b(+) by Gibson assembly using the NEBuilder Assembly Master Mix (NEB). Thus, the resulting genes harbor at the 3′-end a DNA sequence encoding an in-frame C-terminal His tag. The nucleotide sequences of the cloned DNAs were confirmed by Sanger sequencing and the corresponding plasmids were individually transformed into *E. coli* strain BL21 (DE3).

For protein overexpression, bacteria were grown at 37°C in LB medium supplemented with 100 μg ml^{-1} ampicillin. Gene expression was induced by addition of isopropyl b-D-1-thiogalactopyranoside (IPTG; 1 mM final concentration), and cultures were further grown for 3 h. Cells were harvested and washed in Tris-buffered saline (TBS - 50 mM Tris, 138 mM NaCl, 2.7 mM KCl; pH 8.0), and stored at −80°C until protein purification. Cells were lysed by re-suspension in lysis buffer containing 20 mM Tris–HCl, pH 7.4, 300 mM NaCl, 15% glycerol, 1× BugBuster® (Millipore), 1 mg ml^{-1} lysozyme, 25 U ml^{-1} Benzonase® Nuclease (Sigma) and 1× cOmplete™ protease inhibitor (Roche) and incubation on ice for 15 min. The lysate was centrifuged at 7,000 × *g* at 4°C for 30 min. The supernatant was applied to a column containing TALON® metal affinity resin (TaKaRa) for affinity purification of the His-tagged proteins. The column was washed with buffer containing 20 mM Tris–HCl, pH 7.4, 300 mM NaCl and 15% glycerol, and proteins were eluted using the same buffer now containing 250 mM imidazole. The eluted protein was concentrated and buffer-changed to 2× $TAKM_7$ buffer [100 mM Tris–HCl, pH 7.5, 140 mM NH_4Cl, 60 mM KCl, 14 mM $MgCl_2$] by centrifugal ultrafiltration using Amicon Ultra-15 Centrifugal Filters with MW cutoff of 50 K (Millipore); one volume of glycerol was added before protein storage at −20°C.

Preparation of crude *B. thetaiotaomicron* ribosomes

Wild-type *B. thetaiotaomicron* (GT23) was grown in TYG medium to OD_{600} = ~0.6, harvested by centrifugation and washed in cold Ribosome Extraction Buffer [20 mM Tris–HCl, pH 7.5, 50 mM Mg $(OAc)_2$, 100 mM NH_4Cl, 1.0 mM DTT, 0.5 mM ethylenediaminetetraacetic acid (EDTA)] (Rivera *et al*, 2015). The cell pellet was resuspended in Ribosome Extraction Buffer supplemented with 100 μl 10× BugBuster® (Millipore), 1 mg ml^{-1} lysozyme, 1,000 U·ml^{-1} SUPERase·In™ and 10 U ml^{-1} RNase-free DNase I (Roche) and lysed by three cycles of freeze–thaw. The lysate was cleared of cell debris by centrifugation at 20,000 × *g* at 4°C for 30 min. The supernatant was transferred to ultracentrifuge compatible tubes and centrifuged at 100,000 × *g* at 4°C for 1 h to pellet the ribosomes. After removing the supernatant, the crude ribosome pellet was resuspended in buffer containing 20 mM Tris–HCl (pH 7.5), 10 mM Mg $(OAc)_2$, 10 mM KCl and 20 mM NH_4Cl and stored at −80°C. The prepared crude ribosome had poor rRNA integrity likely due to endogenous *B. thetaiotaomicron* RNases. Despite its low *in vitro* protein synthesis activity, the ribosome preparation stimulated GTP hydrolysis by EF-G1 (Fig 2B).

Components of the translation machinery

E. coli ribosomes, f[^{3}H]Met-$tRNA^{fMet}$, [^{14}C]Phe-$tRNA^{Phe}$, [^{14}C]Lys-$tRNA^{Lys}$, Phe-$tRNA^{Phe}$, initiation factors, EF-Tu and *E. coli* EF-G were prepared as described (Peng *et al*, 2019). mRNAs were synthesized by IBA (Goettingen, Germany). The following mRNA sequences were used (start codons are in bold face): mRNA(MKF): 5′-GUUAACAGGUAUACAUACU**AUG**AAAUUCAUUAC-3′; mRNA (MF): 5′-GUUAACAGGUAUACAUACU**AUG**UUUGUUAUUAC-3′.

Ribosome complexes

To prepare initiation complexes (IC), 70S ribosomes were incubated with a 2-fold excess of mRNA, 1.7-fold excess of initiation factors, 3-fold excess of f[^{3}H]Met-$tRNA^{fMet}$, and 1 mM GTP in $TAKM_7$ buffer (50 mM Tris–HCl pH 7.5 at 37°C, 70 mM NH_4Cl, 30 mM KCl and 7 mM $MgCl_2$) at 37°C for 30 min. Ternary complexes (TC) were prepared by incubating EF-Tu (3-fold excess over tRNA) with 1 mM GTP, 3 mM phosphoenolpyruvate, 0.5% pyruvate kinase in $TAKM_7$ buffer at 37°C for 15 min and subsequent addition of aminoacyl-tRNAs cognate to the mRNA coding sequence. Pre-translocation complex (PRE) was formed by mixing IC and TC (2–5-fold excess over IC). Purification of IC and PRE were performed by centrifugation through a 1.1 M sucrose cushion in $TAKM_{21}$ buffer (50 mM Tris–HCl pH 7.5 at 37°C, 70 mM NH_4Cl, 30 mM KCl and 21 mM $MgCl_2$). Pellets were dissolved in $TAKM_{21}$ buffer and the concentration of purified complex was determined by filtration through a nitrocellulose membrane (Peng *et al*, 2019). The magnesium concentration of purified complexes was adjusted to working (7 mM)

 © 2022 The Authors

concentration before use. Experiments were carried out in $TAKM_7$ unless stated otherwise.

Tripeptide synthesis assays

Tripeptide formation was examined by incubation of initiation complex (IC) programmed with mRNA(MKF) (0.1 μM) with TC(Phe-$tRNA^{Phe}$, [^{14}C]Lys-$tRNA^{Lys}$; 0.2 μM each) and EF-G (2 μM) in $TAKM_7$ buffer at 37°C. Samples were taken at 1 and 5 min and quenched by addition of KOH (0.5 μM). Products released from the ribosomes following incubation at 37°C for 30 min were neutralized with glacial acetic acid and analyzed by reversed-phase HPLC (Chromolith®RP-8 e column, Merck) using a 0–65% acetonitrile gradient in 0.1% trifluoroacetic acid. The amounts of fMKF tripeptide was quantified by [^{3}H]Met and [^{14}C]Lys radioactivity counting.

Stopped-Flow translocation experiments

Translocation was measured as described (Peng *et al*, 2019). Pre-translocation complexes programmed with mRNA (mMF) labeled with fluoresceine attached at position + 14 (MF+14Flu; 0.05 μM) and purified by ultracentrifugation through 1.1 M sucrose cushion and mixed with different EF-G proteins (2 μM) along with GTP (200 μM), GDPNP (400 μM) or 200 μM GTP plus 200 μM ppGpp in $TAKM_7$ buffer in a stopped-flow apparatus (SX 20, Applied Photophysics) at 37°C (all concentrations after mixing). Fluorescence was excited at 470 nm and emission detected after passing a KV500 cut-off filter. Changes in fluorescence were recorded with time and 5–7 technical replicates were averaged (n = 5–7). Date was evaluated by double exponential fitting using TableCurve software (Systat Software Inc).

Ribosome recycling experiments

Subunit splitting was measured as described (Savelsbergh *et al*, 2009). Vacant ribosomes (0.05 μM) were rapidly mixed with EF-G (2 μM), RRF (5 μM), IF3 (1 μM), and GTP (1 mM) in $TAKM_7$ buffer in a stopped-flow apparatus (SX 20, Applied Photophysics) at 37°C and light-scattering was monitored at 430 nm (all concentrations after mixing).

Factor-ribosome co-sedimentation assays

Co-sedimentation assays were performed as described (Cunha *et al*, 2013; Wieland *et al*, 2022). Specifically, 0.4 μM of purified *E. coli* 70S were mixed with 1 μM indicated EF-G protein, 500 μM GTP in $TAKM_7$ buffer (50 mM Tris–HCl pH 7.5 at 37°C, 70 mM NH_4Cl, 30 mM KCl and 7 mM $MgCl_2$). Reactions were incubated for 5 min at 20°C, and subsequently loaded on a 10% (w/v) sucrose cushion in $TAKM_7$ and centrifuged for 35 min at 212,911 x g in a TLA100 rotor at 4°C. The pre-centrifugation reactions and 5 pmol of the ribosome pellet (quantified by A260), were applied to NuPAGE 4–12% Bis-Tris protein gel (ThermoFisher) and fractionated at 180 V in 1× MOPS running buffer (ThermoFisher) for 45 min and stained with GelCode Blue Stain (ThermoFisher).

GTP binding assays

Differential radial capillary action of ligand assay (DraCALA; Roelofs *et al*, 2011) was used to detect GTP binding by the EF-G1 and EF-G2 proteins. Purified proteins of specified concentrations (0.02–25 μM) in binding buffer [50 mM Tris–HCl, (pH 7.5), 10 mM $MgCl_2$, 70 mM NH_4Cl, 1 mM dithiothreitol (DTT)] were mixed with ~1.6 nM [α-^{32}P]-labeled GTP and incubated at room temperature for 5 min before spotting 2.5 μl on a dry nitrocellulose membrane (General Electric), where protein and bound ligand are immobilized at the site of contact (forming an "darker" inner circle in the final radiograph, if ligand is bound to protein), whereas free ligand is mobilized by capillary action with the liquid phase (forming a larger outer circle; Roelofs *et al*, 2011). For competition assays, cold nucleotides (GTP or GDP) of specified concentrations (1 mM, 100 μM and 10 μM) were added in the initial mixture containing 25 μM of EF-G1 or EF-G2 and ~1.6 nM [α-^{32}P]-labeled GTP. Spots were air-dried, and radioactivity signals were detected using a Typhoon FLA9000 PhosphorImager. The fraction of ligand bound was calculated as described (Roelofs *et al*, 2011) using the areas and signal intensities of the inner circle (containing bound ligand) and of the outer circle (entire sample) quantified by the ImageJ software. Data were fitted and dissociation constant K_d was estimated using the one site-specific binding model in GraphPad Prism version 9.3.1.

GTPase assays

Ribosome-stimulated GTPase activity assays

Multiple turnover GTPase activity of EF-G proteins was investigated by incubating vacant *E. coli* 70S ribosomes or pre-translocation complexes programmed with mRNA(MF) (0.5 μM) and EF-G (1 μM) together with 1 mM GTP with a trace amount of [γ-^{32}P] GTP at room temperature. At time points indicated in the figures, reactions were quenched by adding the same volume of 40% formic acid. Samples were analyzed by thin-layer chromatography (Polygram CEL 300, Macherey-Nagel) using 0.5 M potassium phosphate (pH 3.5) as mobile phase. Radioactivity was detected using the phosphor screen and analyzed by phosphorimager (Peng *et al*, 2019). For GTPase competition experiments, EF-G1 and EF-G2 were used at the concentrations indicated in the figure legend, and reactions were incubated at room temperature for 5 min, quenched and analyzed.

B. thetaiotaomicron ribosome-stimulated and intrinsic GTPase activity assays

GTPase assays were carried out as described (Palmer *et al*, 2013) in 50 μl reactions containing: 50 mM Tris–HCl, (pH 7.5), 10 mM $MgCl_2$, 70 mM NH_4Cl, 1 mM dithiothreitol (DTT) and 1.8 mM GTP. Different concentrations of the EF-G1 or EF-G2 (between 0 and 0.05 μM) were tested for both intrinsic GTPase activity and vacant ribosome-dependent GTPase activity upon addition of *E. coli* ribosomes (0.2 μM). To test the ability of *B. thetaiotaomicron* ribosomes to stimulate the GTPase activity, reactions were carried out with EF-G1 or EF-G2 (0.2 μM) and crude *B. thetaiotaomicron* ribosomes (0.1 μM as estimated by A260). When testing EF-G1 and EF-G2 variants, we used 0.05 μM protein and 0.2 μM *E. coli* ribosomes. Incubations were carried out at 37°C for 30 min and reactions were stopped by addition of 150 μl of 50 mM EDTA. The amount of GTP hydrolyzed was determined by measuring the amount of the inorganic phosphate liberated using a colorimetric GTPase assay kit (Novus Biologicals) per the manufacturer's directions.

© 2022 The Authors

In vitro protein synthesis assays

In vitro protein synthesis

In vitro protein synthesis was carried out using a custom-made PURExpress® system (New England Biolabs) lacking the *E. coli* EF-G protein, which allowed us to test the behavior of the purified *E. coli* EF-G, *B. thetaiotaomicron* EF-G1 and EF-G2 proteins, and engineered variants. As template, we used linear DNA fragments corresponding to a gene encoding the HslO-FLAG protein or a gene encoding the His-FLAG protein driven by a T7 promoter, generated by PCR using primers listed in Appendix Table S2 with genomic DNA from *Salmonella enterica* serovar Typhimurium strain 14,028 as template (Gao *et al*, 2019). Reaction mixtures taken at different times were added to NuPAGE™ LDS sample buffer (ThermoFisher) containing 100 mM dithiothreitol (DTT) and kept on ice until heated for SDS–PAGE.

Western blot analyses of in vitro synthesized proteins

Samples were heated at 95°C for 5 min, loaded onto a NuPAGE 4–12% Bis-Tris protein gel (ThermoFisher), and fractionated at 180 V in 1× MOPS running buffer (ThermoFisher) for 60 min. Fractionated proteins were transferred to a nitrocellulose membrane using an iBlot device (Invitrogen) and the resulting membrane was blocked in TBS containing 3% skim milk for 1 h. The FLAG-tagged proteins were detected using a 1:5,000 dilution of mouse anti-FLAG antibody (Sigma) followed by a 1:5,000 dilution of an HRP-conjugated anti-mouse antibody (Promega). Between primary and secondary antibody incubations, and after secondary antibody incubation, membranes were washed with TBS containing 0.05% Tween-20 and rinsed with TBS. Blots were developed with SuperSignal West Femto Maximum Sensitivity Substrate (ThermoFisher) and imaged using a LAS-4000 imager (General Electric).

Polysome profiling and fraction analysis

Polysome profiling was carried out as reported (Becker *et al*, 2013). Briefly, *B. thetaiotaomicron* strain WH407 (encoding EF-G1-FLAG and EF-G2-HA) was grown in TYG to OD_{600} = ~0.45, when 100 μg ml^{-1} chloramphenicol was added. Cultures were shaken for 1 min and poured onto crushed chloramphenicol-ice (ice made from ultrapure water with 100 μg ml^{-1} chloramphenicol). Cells were collected by centrifugation at 7,000 × *g* at 4°C for 5 min (Aretakis *et al*, 2018). (The chloramphenicol and centrifugation method was chosen because the *B. thetaiotaomicron* culture rapidly clogged the membrane filter used for ribosome profiling experiments with *Bacillus subtilis* or *E. coli* cells.) Cell pellets were washed in lysis buffer once followed by centrifugation at 7,000 × *g* at 4°C for 5 min and resuspended in lysis buffer before added 100 U ml^{-1} RNase-free DNase I (Roche). The cell suspension was slowly dripped into and frozen in liquid nitrogen, stored at −80°C before lysis. Cells were lysed by cryogenic milling in liquid nitrogen chilled stainless-steel jars using a mixer mill (Retsch, MM400) for five times at 15 Hz for 3 min each time. Jars were chilled in liquid nitrogen in between. Pulverized cells were kept frozen at −80°C before sucrose gradient ultracentrifugation analysis. The lysate was thawed on ice, centrifuged at 20,000 × *g* at 4°C for 10 min to remove insoluble cell debris. The cleared cell lysate (~16 unit of A260) was layered on top of a 10–40% sucrose gradient and subjected to ultracentrifugation at 209,490 x *g* at 4°C for 3 h in a SW41 rotor (Beckman). The gradient was fractionated and the polysome profile (A260) was recorded using a density gradient fractionation system with a UV detector (BRANDEL). Eleven fractions total were collected from each gradient, and proteins from each fraction were extracted using TCA precipitation and analyzed by Western blotting using antibodies directed to the FLAG and HA tags.

Subjecting *B. thetaiotaomicron* to carbon or nitrogen limitation

B. thetaiotaomicron strains were grown in TYG medium anaerobically overnight before being sub-cultured into glucose minimal media (MM; see Bacterial Strains and Growth Conditions). The resulting stationary phase culture was diluted 1:50 into identical pre-reduced medium and grown to mid-exponential phase (OD ~0.5) at which time an aliquot was collected by centrifugation at 7,000 × *g* at room temperature for 1 min. After decanting, the cell pellet was immediate placed on dry ice until the end of the experiment (samples denoted "-5 min"). The remaining culture was centrifuged at 7,000 × *g* at room temperature for 3 min in sealed tubes, re-introduced into the anaerobic chamber where the supernatants were decanted. Cell pellets were resuspended in an equivalent volume of pre-warmed, pre-reduced MM or MM without glucose or $(NH_4)_2SO_4$ ("No C" or "No N" samples in the figure, respectively) and incubated at 37°C anaerobically (Townsend II *et al*, 2020). Following incubation for 15 and 60 min, aliquots were collected by centrifugation, the supernatant was decanted before the pellet was placed on dry ice until storage at −80°C.

Western blot for bacterial extracts

Whole cell lysate preparation

Frozen pellets from 10 ml of exponential phase cells grown in minimal media or equivalent amounts of TYG-cultured cells from different growth stages were used for whole cell lysate preparation. Pellets were thawed and lysed in 300 μl Tris-buffered saline (TBS – 50 mM Tris, 138 mM NaCl, 2.7 mM KCl; pH 8.0) containing 1× BugBuster® (Millipore), 1 mM EDTA, 0.5 mg ml^{-1} chicken egg lysozyme and 25 U·ml^{-1} Benzonase® Nuclease (Sigma), by incubating with constant nutating at room temperature for 20 min. Samples were centrifuged at 20,000 × *g* at 4°C for 10 min to remove cell debris. Protein concentrations were estimated by measuring absorbance at 280 nm using a Nanodrop 8000 (ThermoFisher).

Western blot analysis to detect FLAG-tagged EF-G1 or EF-G2 proteins

A volume corresponding to 100 μg of protein from each sample was combined with 5 μl of 4× LDS Buffer (ThermoFisher) containing 100 mM dithiothreitol and subjected to heating at 95°C for 5 min. Samples were loaded onto a NuPAGE 4–12% Bis-Tris protein gel (ThermoFisher) and fractionated at 180 V in 1× MOPS running buffer (ThermoFisher) for 60 min. Fractionated proteins were transferred to a nitrocellulose membrane using an iBlot device (Invitrogen) and the resulting membrane was cut below the 65 kDa marker and both portions blocked in TBS containing 3% skim milk for 1 h. FLAG-tagged EF-G2 was detected on the top portion of the membrane using a 1:5,000 dilution of a mouse anti-FLAG antibody (Sigma) followed by incubation with a 1:5,000 dilution of an HRP-

 © 2022 The Authors

conjugated anti-mouse antibody (Promega). GroEL was detected on the bottom portion of the membrane using a 1:5,000 dilution of rabbit anti-GroEL antibody (Sigma) followed by incubation with a 1:5,000 dilution of an HRP-conjugated anti-rabbit antibody (General Electric). Between primary and secondary antibody incubations, and after secondary antibody incubation, membranes were washed with TBS containing 0.05% Tween-20 and rinsed with TBS. Blots were developed with SuperSignal West Femto Maximum Sensitivity Substrate (ThermoFisher) and imaged using a LAS-4000 imager (General Electric).

Mouse gut colonization experiments

Inoculum preparation

Overnight cultures of barcoded *B. thetaiotaomicron* strains grown separately in TYG medium anaerobically overnight were diluted 1:50 into fresh TYG and cultured individually for 8 h. Bacteria were collected by centrifugation and resuspended in TYG containing 20% glycerol and divided into identical aliquots before storage at −80°C. Density of each strain stock was measured by thawing one aliquot and plating for CFUs after serial dilution.

Mono-colonization experiments

10^8 CFUs were suspended in 200 μl phosphate-buffered saline and administered to each animal by oral gavage. Mice were euthanized 4 days after gavage and cecal contents were collected as ~100 mg aliquots, flash frozen in liquid nitrogen, and stored at −80°C before RNA or protein extraction.

In vivo competition experiments

10^8 CFUs of each strain (wild-type, GT478; *ΔBT2167*, WH148; *ΔBT2167 + BT2167*, WH160; *ΔBT2167 + BT2167(H593K)*, WH514) were combined and suspended in 200 μl phosphate-buffered saline before administering to each animal by oral gavage. Input (day 0) abundance of each strain was determined by plating and counting the CFUs of each strain stock after serial dilution. Fecal pellets were collected on the indicated days and genomic DNA was extracted as described (Martens *et al*, 2008). The abundance of each strain was measured by qPCR, using barcode-specific primers (wild-type, primers W1701 and W1713; *ΔBT2167*, primers W1702 and W1713; *ΔBT2167 + BT2167*, primers W1712 and W1713; or *ΔBT2167 + BT2167(H593K)*, primers W1711 and W1713) as described (Martens *et al*, 2008).

Western blot for bacteria from murine gut

Cecal bacterial lysate preparation

~100 mg of cecal content was well-suspended in 10 ml cold TBS and centrifuged at 300 × *g* at 4°C for 1 min. The supernatant was transferred to a new tube and bacteria were pelleted by centrifuging at 7,000 × *g* at 4°C for 5 min. Cell pellets were then washed with 1 ml cold TBS, re-suspended and lysed in 400 μl cold TBS containing 1× BugBuster® (Millipore), 1 mM EDTA, 0.5 mg ml^{-1} chicken egg lysozyme, 25 U ml^{-1} Benzonase® nuclease (Sigma) and 1× cOmplete™ protease inhibitor, by incubating with constant nutating at 4°C for 10 min. Samples were centrifuged at 20,000 × *g* at 4°C for 10 min to remove cell debris. Protein concentrations were estimated by measuring absorbance at 280 nm using a Nanodrop 8000 (ThermoFisher).

Western blot detection of wild-type (i.e., untagged) EF-G1 and EF-G2 proteins

A volume corresponding to 50 μg of protein from each cecal sample was combined with 5 μl 4 × LDS Buffer (ThermoFisher) containing 100 mM dithiothreitol and incubated at 95°C for 5 min. Samples were loaded onto a NuPAGE 4–12% Bis-Tris protein gel (ThermoFisher) and fractionated at 180 V in 1× MOPS running buffer (ThermoFisher) for 60 min. Fractionated proteins were transferred to a nitrocellulose membrane using an iBlot device (Invitrogen) and the resulting membrane was cut below the 65 kD marker and both portions blocked in TBS containing 3% skim milk for 1 h. The EF-G1 and EF-G2 proteins were detected at the top portion of the membrane using a 1:1,000 dilution of the rabbit anti-EF-G1 antiserum (day-56 bleed) or 1:5,000 dilution of the rabbit anti-EF-G2 antiserum (day-56 bleed), followed by a 1:5,000 dilution of an HRP-conjugated anti-rabbit antibody (General Electric). GroEL was detected on the bottom portion of the membrane using a 1:5,000 dilution of anti-GroEL (Sigma) followed by incubation with a 1:5,000 dilution of an HRP-conjugated anti-rabbit antibody (General Electric). Between primary and secondary antibody incubations, and after secondary antibody incubation, membranes were washed with TBS containing 0.05% Tween-20 and rinsed with TBS. Blots were developed with SuperSignal West Femto Maximum Sensitivity Substrate (ThermoFisher) and imaged using a LAS-4000 imager (General Electric).

Cryo-EM structure analysis

Cryo-EM sample preparation

For Cryo-EM grid preparation, we mixed *E. coli* ribosomes (1.6 μM), EF-G2 (5.2 μM), and GTP (2.5 mM) in buffer containing 50 mM Tris–HCl pH 7.5, 10 mM $MgCl_2$ and 70 mM NH_4Cl at room temperature. A total of 5 μl of the samples was applied onto glow-discharged (40 s) 200-mesh R2/1 Quanti-foil Cu grids with 2 nm thick continuous carbon film. The grids were blotted for 3 s manually and rapidly frozen in liquid ethane using a home-made plunger.

Cryo-EM single-particle data acquisition

The frozen grids were loaded into a Titan Krios (ThermoFisher) operated at 300 kV, condenser lens aperture 50 μm, spot size 7, parallel beam with illuminated area of 1.25 μm in diameter. Microscope magnification was at 81,000× (corresponding to a calibrated sampling of 1.068 Å per physical pixel). Movie stacks were collected automatically using Serial-EM software on a K3 direct electron camera equipped with a GIF quantum energy filter (Gatan) with a slit width of 20 eV to remove inelastically scattered electrons. Images are collected in super-resolution mode at a recording rate of 40 raw frames per second and a total exposure time of 2 s, yielding 40 frames per image stack, and a total dose of 30 $e-/Å^2$. Totally, ~10,720 micrographs were collected automatically using Serial-EM (Mastronarde, 2005) with defocus values ranging between −0.6 and −2 μm.

Cryo-EM data processing and model building

Movie stacks were motion-corrected using Motioncor2 (Zheng *et al*, 2017). After CTF correction by Gctf (Zhang, 2016), Relion (Scheres, 2016) were used to pick particles. After 2d classification and 3d classification, ~342,233 particles contributing to the 70S ribosome reconstruction were sorted out. This group of particles were further classified into two classes: 70S ribosome without and with

© 2022 The Authors

EF-G2 associated. To improve the resolution of the EF-G2 associated with the ribosome, we subtracted the EF-G2 density map from the raw images and carried out focused refinement, which generated a density map with a global resolution of 4 Å estimated using 0.143FSC standard. To analyze the different conformations of the 70S-EF-G2, we performed 3d classification on this group of particles.

After 3d classification, 40,595 and 93,541 particles contributing to the two best-resolved classes from the 70S-EF-G2 group were subjected to further 3d refinement, which generates the two density maps with a global resolution of 3.2 and 3.0 Å, respectively.

To better visualize the interaction between the EF-G2 and SRL, we applied local mask around this region for 3d refinement. After 3d classification, the best class contributed by 63,782 particles was subjected to further refinement, which generates a density map with local resolution of the EF-G2-SRL region around 3.7 Å. To build atomic model of the EF-G2 associated with the ribosome, we first ran AlphaFold2 (Jumper *et al*, 2021) to obtain predicated model, which was fitted into the focused refined EF-G2 density map first and then refined in Phenix (Afonine *et al*, 2018). The refined model was manually adjusted based on our density map in Coot (Emsley *et al*, 2010). To build the models of the two refined classes from the 70S-EF-G2 complexes, we extracted the models of the 70S from the released models (PDB: 7ST6 and 7SSD) and combined them with our refined EF-G2 model respectively. The composed models were then fitted into the two density maps and refined in real space using Phenix respectively (Appendix Fig S1). All structures were visualized using Chimera (Pettersen *et al*, 2004) or Chimera X (Pettersen *et al*, 2021).

Bioinformatic analyses

Bacteroidetes genome analysis was carried out using PATRIC (Davis *et al*, 2020); phylogenetic tree and data were visualized using iTOL (Letunic & Bork, 2021). The 149 *Bacteroidetes* genomes available for building the *Bacteroidale* order level pre-built tree in PATRIC were first analyzed for the presence and conservation of EF-G1 and EF-G2 by tBLASTn, using *B. thetaiotaomicron* EF-G1 or EF-G2 as query sequences. The resulted hits that share more identity with EF-G1 or EF-G2 were considered as EF-G1- or EF-G2- orthologs, respectively. More fully sequenced genomes from *Bacteroidetes* outside the *Bacteroidia* class were randomly picked for analyzing the presence of EF-G1 and EF-G2 using the same tBLASTn method.

Protein sequence alignments were carried out by MUSCLE (Edgar, 2004) and Clustal Omega (Sievers *et al*, 2011). For analyzing sequence conservation in non-redundant *Bacteroides* EF-G1/EF-G2 proteins, all proteins entries with annotations containing key words 'elongation factor G', 'EF-G' or 'fusA', and '*Bacteroides*' were retrieved from NCBI identical protein groups, aligned using MUSCLE and built distance tree using PHYLIP (Felsenstein, 2005), proteins on the same clade as *B. thetaiotaomicron* EF-G1 or EF-G2 were considered as EF-G1- or EF-G2- ortholog proteins, respectively, and sequence logos were built using WebLogo 3 (Crooks *et al*, 2004).

Data availability

The atomic coordinates and cryo-EM 3D maps for protein structures produced in this study are available through the Protein Data Bank (PDB) and the Electron Microscopy Data Bank (EMDB), respectively, as follows:

- focused refined EF-G2: PDB 8DMF (http://www.rcsb.org/pdb/explore/explore.do?structureId=8DMF);
- focused refined EF-G2: EMD-27535
- 70 S-EF-G2 complex: EMD-27561
- Class 1 of 70 S-EF-G2 complex: EMD-27543
- Class 2 of 70 S-EF-G2 complex: EMD-27546
- Local refined density map including SRL-EF-G2 region: EMD-27547

Expanded View for this article is available online.

Acknowledgements
We would like to thank Peter Moore and Alexander Mankin for discussions; Tanel Tenson, Jonathan Dworkin, Allen Buskirk, and Jennifer Aronson for comments on the manuscript; Jack Chun-Chieh Hsu, Lizamarie Valle and Diane Lazo for technical advice and support and Olaf Geintzer, Vanessa Herold, Tessa Hübner, Franziska Hummel, Sandra Kappler, Christina Kothe, Anna Pfeifer, Theresia Steiger, and Michael Zimmermann for expert technical assistance. This work is supported by the grants R01 GM123798 (to EAG), R35 GM1181579 (to ALG) and R01 GM110243 (to JL) from the National Institutes of Health and grant of the Deutsche Forschungsgemeinschaft (Leibniz Prize to MVR).

Author contributions
Weiwei Han: Conceptualization; formal analysis; investigation; writing – original draft; writing – review and editing. **Bee-Zen Peng:** Formal analysis; investigation. **Chunyan Wang:** Formal analysis; investigation; visualization. **Guy E Townsend II:** Investigation; writing – review and editing. **Natasha A Barry:** Resources. **Frank Peske:** Conceptualization; resources; formal analysis; investigation; methodology. **Andrew L Goodman:** Resources; funding acquisition. **Jun Liu:** Supervision; funding acquisition. **Marina V Rodnina:** Resources; formal analysis; supervision; funding acquisition; methodology; writing – review and editing. **Eduardo A Groisman:** Conceptualization; formal analysis; funding acquisition; writing – original draft; project administration; writing – review and editing.

Disclosure and competing interests statement
The authors declare that they have no conflict of interest.

References

Afonine PV, Poon BK, Read RJ, Sobolev OV, Terwilliger TC, Urzhumtsev A, Adams PD (2018) Real-space refinement in PHENIX for cryo-EM and crystallography. *Acta Crystallogr D Struct Biol* 74: 531 – 544

Aretakis JR, Al-Husini N, Schrader JM (2018) Methodology for ribosome profiling of key stages of the *Caulobacter crescentus* cell cycle. *Methods Enzymol* 612: 443 – 465

Atkinson GC (2015) The evolutionary and functional diversity of classical and lesser-known cytoplasmic and organellar translational GTPases across the tree of life. *BMC Genomics* 16: 78

Becker AH, Oh E, Weissman JS, Kramer G, Bukau B (2013) Selective ribosome profiling as a tool for studying the interaction of chaperones and targeting factors with nascent polypeptide chains and ribosomes. *Nat Protoc* 8: 2212 – 2239

Belardinelli R, Sharma H, Caliskan N, Cunha CE, Peske F, Wintermeyer W, Rodnina MV (2016) Choreography of molecular movements during ribosome progression along mRNA. *Nat Struct Mol Biol* 23: 342 – 348

 © 2022 The Authors

Belitsina NV, Glukhova MA, Spirin AS (1975) Translocation in ribosomes by attachment-detachment of elongation-factor G without Gtp cleavage – evidence from a column-bound ribosome system. *FEBS Lett* 54: 35 – 38

Belitsina NV, Glukhova MA, Spirin AS (1976) Stepwise elongation factor G-promoted elongation of polypeptides on the ribosome without GTP cleavage. *J Mol Biol* 108: 609 – 613

Carbone CE, Loveland AB, Gamper HB Jr, Hou YM, Demo G, Korostelev AA (2021) Time-resolved cryo-EM visualizes ribosomal translocation with EF-G and GTP. *Nat Commun* 12: 7236

Cashel M, Gallant J (1969) Two compounds implicated in the function of the RC gene of *Escherichia coli*. *Nature* 221: 838 – 841

Clementi N, Chirkova A, Puffer B, Micura R, Polacek N (2010) Atomic mutagenesis reveals A2660 of 23 S ribosomal RNA as key to EF-G GTPase activation. *Nat Chem Biol* 6: 344 – 351

Connell SR, Takemoto C, Wilson DN, Wang H, Murayama K, Terada T, Shirouzu M, Rost M, Schuler M, Giesebrecht J *et al* (2007) Structural basis for interaction of the ribosome with the switch regions of GTP-bound elongation factors. *Mol Cell* 25: 751 – 764

Corrigan RM, Bellows LE, Wood A, Grundling A (2016) ppGpp negatively impacts ribosome assembly affecting growth and antimicrobial tolerance in gram-positive bacteria. *Proc Natl Acad Sci USA* 113: E1710 – E1719

Crooks GE, Hon G, Chandonia JM, Brenner SE (2004) WebLogo: a sequence logo generator. *Genome Res* 14: 1188 – 1190

Cunha CE, Belardinelli R, Peske F, Holtkamp W, Wintermeyer W, Rodnina MV (2013) Dual use of GTP hydrolysis by elongation factor G on the ribosome. *Translation (Austin)* 1: e24315

Davis JJ, Wattam AR, Aziz RK, Brettin T, Butler R, Butler RM, Chlenski P, Conrad N, Dickerman A, Dietrich EM *et al* (2020) The PATRIC Bioinformatics Resource Center: expanding data and analysis capabilities. *Nucleic Acids Res* 48: D606 – D612

Diez S, Ryu J, Caban K, Gonzalez RL, Dworkin J (2020) The alarmones (p) ppGpp directly regulate translation initiation during entry into quiescence. *Proc Natl Acad Sci USA* 117: 15565 – 15572

Donaldson GP, Lee SM, Mazmanian SK (2016) Gut biogeography of the bacterial microbiota. *Nat Rev Microbiol* 14: 20 – 32

Dykhuizen D, Hartl DL (1980) Selective neutrality of 6PGD allozymes in *E. coli* and the effects of genetic background. *Genetics* 96: 801 – 817

Edgar RC (2004) MUSCLE: multiple sequence alignment with high accuracy and high throughput. *Nucleic Acids Res* 32: 1792 – 1797

Emsley P, Lohkamp B, Scott WG, Cowtan K (2010) Features and development of coot. *Acta Crystallogr D Biol Crystallogr* 66: 486 – 501

Felsenstein J (2005) *PHYLIP (phylogeny inference package) version 3.6. Distributed by the author*. Seattle, WA: Department of Genome Sciences, University of Washington

Gao YG, Selmer M, Dunham CM, Weixlbaumer A, Kelley AC, Ramakrishnan V (2009) The structure of the ribosome with elongation factor G trapped in the posttranslocational state. *Science* 326: 694 – 699

Gao X, Yeom J, Groisman EA (2019) The expanded specificity and physiological role of a widespread N-degron recognin. *Proc Natl Acad Sci USA* 116: 18629 – 18637

Goodman AL, McNulty NP, Zhao Y, Leip D, Mitra RD, Lozupone CA, Knight R, Gordon JI (2009) Identifying genetic determinants needed to establish a human gut symbiont in its habitat. *Cell Host Microbe* 6: 279 – 289

Haseltine WA, Block R, Gilbert W, Weber K (1972) MSI and MSII made on ribosome in idling step of protein synthesis. *Nature* 238: 381 – 384

Hirashima A, Kaji A (1973) Role of elongation factor G and a protein factor on the release of ribosomes from messenger ribonucleic acid. *J Biol Chem* 248: 7580 – 7587

Holdeman LV, Cato EP, Moore WE (1977) *Anaerobe laboratory manual*. Blacksburg, VA: Virginia Polytechnic Institute and State University Anaerobe Laboratory

Holtkamp W, Cunha CE, Peske F, Konevega AL, Wintermeyer W, Rodnina MV (2014) GTP hydrolysis by EF-G synchronizes tRNA movement on small and large ribosomal subunits. *EMBO J* 33: 1073 – 1085

Inoue-Yokosawa N, Ishikawa C, Kaziro Y (1974) The role of guanosine triphosphate in translocation reaction catalyzed by elongation factor G. *J Biol Chem* 249: 4321 – 4323

Jumper J, Evans R, Pritzel A, Green T, Figurnov M, Ronneberger O, Tunyasuvunakool K, Bates R, Zidek A, Potapenko A *et al* (2021) Highly accurate protein structure prediction with AlphaFold. *Nature* 596: 583 – 589

Kaziro Y (1978) The role of guanosine 5′-triphosphate in polypeptide chain elongation. *Biochim Biophys Acta* 505: 95 – 127

Kimura M (1983) *The neutral theory of molecular evolution*. Cambridge: Cambridge University Press

Koropatkin NM, Martens EC, Gordon JI, Smith TJ (2008) Starch catabolism by a prominent human gut symbiont is directed by the recognition of amylose helices. *Structure* 16: 1105 – 1115

Kuriki Y, Inoue N, Kaziro Y (1970) Formation of a complex between GTP, G factor, and ribosomes as an intermediate of ribosome-dependent GTPase reaction. *Biochim Biophys Acta* 224: 487 – 497

La Rosa SL, Ostrowski MP, Vera-Ponce de Leon A, McKee LS, Larsbrink J, Eijsink VG, Lowe EC, Martens EC, Pope PB (2022) Glycan processing in gut microbiomes. *Curr Opin Microbiol* 67: 102143

Letunic I, Bork P (2021) Interactive Tree Of Life (iTOL) v5: an online tool for phylogenetic tree display and annotation. *Nucleic Acids Res* 49: W293 – W296

Ley RE, Hamady M, Lozupone C, Turnbaugh PJ, Ramey RR, Bircher JS, Schlegel ML, Tucker TA, Schrenzel MD, Knight R *et al* (2008) Evolution of mammals and their gut microbes. *Science* 320: 1647 – 1651

Li W, Liu Z, Koripella RK, Langlois R, Sanyal S, Frank J (2015) Activation of GTP hydrolysis in mRNA-tRNA translocation by elongation factor G. *Sci Adv* 1: e1500169

Li SH, Li Z, Park JO, King CG, Rabinowitz JD, Wingreen NS, Gitai Z (2018) *Escherichia coli* translation strategies differ across carbon, nitrogen and phosphorus limitation conditions. *Nat Microbiol* 3: 939 – 947

Margus T, Remm M, Tenson T (2011) A computational study of elongation factor G (EFG) duplicated genes: diverged nature underlying the innovation on the same structural template. *PLoS ONE* 6: e22789

Martens EC, Chiang HC, Gordon JI (2008) Mucosal glycan foraging enhances fitness and transmission of a saccharolytic human gut bacterial symbiont. *Cell Host Microbe* 4: 447 – 457

Martens EC, Kelly AG, Tauzin AS, Brumer H (2014) The devil lies in the details: How variations in polysaccharide fine-structure impact the physiology and evolution of gut microbes. *J Mol Biol* 426: 3851 – 3865

Mastronarde DN (2005) Automated electron microscope tomography using robust prediction of specimen movements. *J Struct Biol* 152: 36 – 51

Mitkevich VA, Ermakov A, Kulikova AA, Tankov S, Shyp V, Soosaar A, Tenson T, Makarov AA, Ehrenberg M, Hauryliuk V (2010) Thermodynamic characterization of ppGpp binding to EF-G or IF2 and of initiator tRNA binding to free IF2 in the presence of GDP, GTP, or ppGpp. *J Mol Biol* 402: 838 – 846

Noller HF, Lancaster L, Zhou J, Mohan S (2017) The ribosome moves: RNA mechanics and translocation. *Nat Struct Mol Biol* 24: 1021 – 1027

Palmer SO, Rangel EY, Hu Y, Tran AT, Bullard JM (2013) Two homologous EF-G proteins from Pseudomonas aeruginosa exhibit distinct functions. *PLoS ONE* 8: e80252

© 2022 The Authors

Pausch P, Steinchen W, Wieland M, Klaus T, Freibert SA, Altegoer F, Wilson DN, Bange G (2018) Structural basis for (p)ppGpp-mediated inhibition of the GTPase RbgA. *J Biol Chem* 293: 19699 – 19709

Peng BZ, Bock LV, Belardinelli R, Peske F, Grubmuller H, Rodnina MV (2019) Active role of elongation factor G in maintaining the mRNA reading frame during translation. *Sci Adv* 5: eaax8030

Peske F, Rodnina MV, Wintermeyer W (2005) Sequence of steps in ribosome recycling as defined by kinetic analysis. *Mol Cell* 18: 403 – 412

Petrychenko V, Peng BZ, Schwarzer ACAP, Peske F, Rodnina MV, Fischer N (2021) Structural mechanism of GTPase-powered ribosome-tRNA movement. *Nat Commun* 12: 5933

Pettersen EF, Goddard TD, Huang CC, Couch GS, Greenblatt DM, Meng EC, Ferrin TE (2004) UCSF Chimera—a visualization system for exploratory research and analysis. *J Comput Chem* 25: 1605 – 1612

Pettersen EF, Goddard TD, Huang CC, Meng EC, Couch GS, Croll TI, Morris JH, Ferrin TE (2021) UCSF ChimeraX: structure visualization for researchers, educators, and developers. *Protein Sci* 30: 70 – 82

Pulk A, Cate JH (2013) Control of ribosomal subunit rotation by elongation factor G. *Science* 340: 1235970

Raghavan V, Lowe EC, Townsend GE 2nd, Bolam DN, Groisman EA (2014) Tuning transcription of nutrient utilization genes to catabolic rate promotes growth in a gut bacterium. *Mol Microbiol* 93: 1010 – 1025

Rivera MC, Maguire B, Lake JA (2015) Isolation of ribosomes and polysomes. *Cold Spring Harb Protoc* 2015: 293 – 299

Rodnina MV, Savelsbergh A, Katunin VI, Wintermeyer W (1997) Hydrolysis of GTP by elongation factor G drives tRNA movement on the ribosome. *Nature* 385: 37 – 41

Rodnina MV, Peske F, Peng BZ, Belardinelli R, Wintermeyer W (2019) Converting GTP hydrolysis into motion: versatile translational elongation factor G. *Biol Chem* 401: 131 – 142

Roelofs KG, Wang J, Sintim HO, Lee VT (2011) Differential radial capillary action of ligand assay for high-throughput detection of protein-metabolite interactions. *Proc Natl Acad Sci USA* 108: 15528 – 15533

Rojas AM, Ehrenberg M, Andersson SG, Kurland CG (1984) ppGpp inhibition of elongation factors Tu, G and Ts during polypeptide synthesis. *Mol Gen Genet* 197: 36 – 45

Rundlet EJ, Holm M, Schacherl M, Natchiar SK, Altman RB, Spahn CMT, Myasnikov AG, Blanchard SC (2021) Structural basis of early translocation events on the ribosome. *Nature* 595: 741 – 745

Saito K, Kratzat H, Campbell A, Buschauer R, Burroughs AM, Berninghausen O, Aravind L, Green R, Beckmann R, Buskirk AR (2022) Ribosome collisions induce mRNA cleavage and ribosome rescue in bacteria. *Nature* 603: 503 – 508

Salsi E, Farah E, Ermolenko DN (2016) EF-G activation by phosphate analogs. *J Mol Biol* 428: 2248 – 2258

Savelsbergh A, Matassova NB, Rodnina MV, Wintermeyer W (2000) Role of domains 4 and 5 in elongation factor G functions on the ribosome. *J Mol Biol* 300: 951 – 961

Savelsbergh A, Katunin VI, Mohr D, Peske F, Rodnina MV, Wintermeyer W (2003) An elongation factor G-induced ribosome rearrangement precedes tRNA-mRNA translocation. *Mol Cell* 11: 1517 – 1523

Savelsbergh A, Rodnina MV, Wintermeyer W (2009) Distinct functions of elongation factor G in ribosome recycling and translocation. *RNA* 15: 772 – 780

Scheres SH (2016) Processing of structurally heterogeneous Cryo-EM data in RELION. *Methods Enzymol* 579: 125 – 157

Schofield WB, Zimmermann-Kogadeeva M, Zimmermann M, Barry NA, Goodman AL (2018) The stringent response determines the ability of a commensal bacterium to survive starvation and to persist in the gut. *Cell Host Microbe* 24: 120 – 132

Schwalm ND III, Groisman EA (2017) Navigating the gut buffet: control of polysaccharide utilization in *Bacteroides* spp. *Trends Microbiol* 25: 1005 – 1015

Schwalm ND III, Townsend GE II, Groisman EA (2016) Multiple Signals Govern Utilization of a Polysaccharide in the Gut Bacterium *Bacteroides thetaiotaomicron*. *mBio* 7: e01342-16

Sender R, Fuchs S, Milo R (2016) Revised estimates for the number of human and bacteria cells in the body. *PLoS Biol* 14: e1002533

Shi X, Khade PK, Sanbonmatsu KY, Joseph S (2012) Functional role of the sarcin-ricin loop of the 23 S rRNA in the elongation cycle of protein synthesis. *J Mol Biol* 419: 125 – 138

Sievers F, Wilm A, Dineen D, Gibson TJ, Karplus K, Li WZ, Lopez R, McWilliam H, Remmert M, Soding J *et al* (2011) Fast, scalable generation of high-quality protein multiple sequence alignments using Clustal omega. *Mol Syst Biol* 7: 539

Subramaniam AR, Zid BM, O'Shea EK (2014) An integrated approach reveals regulatory controls on bacterial translation elongation. *Cell* 159: 1200 – 1211

Suematsu T, Yokobori S, Morita H, Yoshinari S, Ueda T, Kita K, Takeuchi N, Watanabe Y (2010) A bacterial elongation factor G homologue exclusively functions in ribosome recycling in the spirochaete *Borrelia burgdorferi*. *Mol Microbiol* 75: 1445 – 1454

Tourigny DS, Fernandez IS, Kelley AC, Ramakrishnan V (2013) Elongation factor G bound to the ribosome in an intermediate state of translocation. *Science* 340: 1235490

Townsend GE II, Han W, Schwalm ND III, Hong X, Bencivenga-Barry NA, Goodman AL, Groisman EA (2020) A master regulator of *Bacteroides thetaiotaomicron* gut colonization controls carbohydrate utilization and an alternative protein synthesis factor. *mBio* 11: e03221-19

Vinogradova DS, Zegarra V, Maksimova E, Nakamoto JA, Kasatsky P, Paleskava A, Konevega AL, Milon P (2020) How the initiating ribosome copes with ppGpp to translate mRNAs. *PLoS Biol* 18: e3000593

Voorhees RM, Schmeing TM, Kelley AC, Ramakrishnan V (2010) The mechanism for activation of GTP hydrolysis on the ribosome. *Science* 330: 835 – 838

Wexler AG, Goodman AL (2017) An insider's perspective: Bacteroides as a window into the microbiome. *Nat Microbiol* 2: 17026

Wieland M, Holm M, Rundlet EJ, Morici M, Koller TO, Maviza TP, Pogorevc D, Osterman IA, Muller R, Blanchard SC *et al* (2022) The cyclic octapeptide antibiotic argyrin B inhibits translation by trapping EF-G on the ribosome during translocation. *Proc Natl Acad Sci USA* 119: e2114214119

Wu M, McNulty NP, Rodionov DA, Khoroshkin MS, Griffin NW, Cheng J, Latreille P, Kerstetter RA, Terrapon N, Henrissat B *et al* (2015) Genetic determinants of in vivo fitness and diet responsiveness in multiple human gut *Bacteroides*. *Science* 350: aac5992

Zhang JZ (2003) Evolution by gene duplication: an update. *Trends Ecol Evol* 18: 292 – 298

Zhang K (2016) Gctf: real-time CTF determination and correction. *J Struct Biol* 193: 1 – 12

Zheng SQ, Palovcak E, Armache JP, Verba KA, Cheng Y, Agard DA (2017) MotionCor2: anisotropic correction of beam-induced motion for improved cryo-electron microscopy. *Nat Methods* 14: 331 – 332

Zhou J, Lancaster L, Donohue JP, Noller HF (2013) Crystal structures of EF-G-ribosome complexes trapped in intermediate states of translocation. *Science* 340: 1236086

 © 2022 The Authors